DISSERTATIONES
PHYSICAE
UNIVERSITATIS
TARTUENSIS
111

VIKTORIIA LEVUSHKINA

Energy transfer processes in the solid solutions of complex oxides

DISSERTATIONES PHYSICAE UNIVERSITATIS TARTUENSIS

111

DISSERTATIONES PHYSICAE UNIVERSITATIS TARTUENSIS
111

VIKTORIIA LEVUSHKINA

Energy transfer processes in the solid solutions of complex oxides

UNIVERSITY OF TARTU
Press

Institute of Physics, Faculty of Science and Technology, University of Tartu, Estonia.

The dissertation was admitted on 04.04.2017 in partial fulfilment of the requirements for the degree of Doctor of Philosophy in Physics, and was allowed for defense by the Council of the Institute of Physics, University of Tartu.

Supervisors: Dr. Dmitry Spassky
Skobeltsyn Institute of Nuclear Physics, M.V. Lomonosov Moscow State University, Russia

Prof., Dr. hab. Mikhail G. Brik
Institute of Physics, University of Tartu, Estonia

Opponent: Dr. Vladimir Makhov
Institute of Physics, Russian Academy of Science, Moscow, Russia

Defense: June 15, 2017 at University of Tartu, Estonia

The studies was supported by Marie Curie Initial Training Network LUMINET (grant agreement no. 316906) and partially by the Estonian Centre of Excellence TK141 by the EU through the European Regional Development Fund (TK141 "Advanced materials and high-technology devices for energy recuperation systems", project No. 2014-2020.4.01.15-0011).

ISSN 1406-0647
ISBN 978-9949-77-438-8 (print)
ISBN 978-9949-77-439-5 (pdf)

University of Tartu Press
www.tyk.ee

CONTENTS

LIST OF PUBLICATIONS INCLUDED IN THE THESIS

I. **Levushkina, V.S.**; Spassky, D.A.; Brik, M.G.; Zych, E.; Madej, A; Belsky, A.N; Bartosiewicz, K.; Nikl, M. Mixed vanadates: optimization of optical properties by varying chemical composition. Journal of Luminescence, in Press. DOI: 10.1016/j.jlumin.2016.12.009.

II. **Levushkina, V.S.**; Spassky, D.A.; Aleksanyan, E.M.; Brik, M.G.; Tretyakova, M.S.; Zadneprovski, B.I.; Belsky, A.N. Bandgap engineering of the $Lu_xY_{1-x}PO_4$ mixed crystals. Journal of Luminescence, 171; 2016, 33–39.

III. **Levushkina, V.S.**; Mikhailin, V.V.; Spassky, D.A.; Zadneprovski, B. I.; Tret'yakova, M.S. Luminescence properties of solid solutions of borates doped with rare-earths ions. Physics of the Solid State, 56(11); 2014, 2247–2258.

IV. Spassky, D.A.; **Levushkina, V.S.**; Mikhailin, V.V.; Zadneprovski, B. I.; Tret'yakova, M.S. Luminescence of Borates with Yttrium and Lutetium Cations. Physics of the Solid State, 55(1); 2013, 150–159.

Author's contribution

Publication I.	The main author of all sections. Material preparation, participation in the experimental work and data processing, manuscript preparation.
Publication II.	Participation in the experimental work and data processing; writing the main part of the manuscript.
Publication III.	Participation in the experimental work and data processing, preparation of figures and manuscript writing.
Publication IV.	Processing and analysis of the experimental data. Participation in the preparation of figures and manuscript writing.

ABBREVIATION

UV	ultraviolet
VUV	vacuum ultraviolet
IR	infra-red
SR	synchrotron radiation
XRD	X-ray diffraction
TSL	thermally stimulated luminescence
e	electron
h	hole
ex	exciton
CB	conduction band
VB	valence band
E_g	bandgap value
E_A	activation energy
SEM	scanning electron microscope
STE	self-trapped exciton
CCD	charged coupled device
RE	rare earth

1. INTRODUCTION

Inorganic compounds based on complex oxides find numerous applications in different fields, for example in medicine, security, fundamental physics, illumination etc [1-4]. Great efforts are constantly being made to develop new materials or improve the targeted properties of already existing ones. The development of compounds with the desired optimal characteristics for the light emitting applications requires detailed knowledge of their electronic and crystal structures along with the peculiarities of the excitation energy transfer to emitting centers. Furthermore, detailed investigation of the origin of emitting centers and defects, which are created during the samples synthesis, is needed for deeper understanding and further improvement of the phosphor properties. Formation of those defects usually prevents the energy transfer to emitting centers, thus resulting in the light output decrease.

Development of the solid solutions is one of possible ways to tune the luminescent and scintillation properties. Substitutional solid solutions (or mixed crystals) are formed when the difference between the ionic radii of substitutional ions is less than 15% and the ions have the same charge. The change of the relative concentration of the substitutional ions leads to variation of the physical properties of solid solutions. For example, the bandgap modification allows to reduce negative influence of the defects on the luminescent properties [5, 6].

Moreover, the luminescence light output was shown to depend non-linearly on the relative concentration of substitutional ions. In many solid solutions the light output was found to be increased in comparison to pure compounds making a given solid solution. Such behavior was observed in $(Lu_xY_{1-x})AlO_3$:Ce [7], $Y_3(Al_xGa_{1-x})_5O_{12}$:Ce [8], $(Lu_xGd_{1-x})_2SiO_5$:Ce [9], $(Lu_xSc_{1-x})BO_3$:Ce [10], $(Lu_xGd_{1-x})_3(Al_yGa_{1-y})_5O_{12}$:Ce [11], BaIBr:Eu [12], $Zn_xMg_{1-x}WO_4$ [13].

It is supposed that this effect can be associated with the limitation of the migration distance between the thermalized genetic electron-hole pairs. The effect may arise due to clusterization in the solid solutions [14], acceleration of thermalization rate by increasing the number of phonon branches [15], or localization of the thermalized charge carriers in the local energy wells at the bottom of the conduction band (CB) and/or the top of the valence band (VB) [16].

The change of light output in the solid solutions can also be caused by other reasons, e.g. structural inhomogeneity (co-existence of several crystalline phases in a particular solid solution), modification of non-radiative relaxation channels (for example, traps, competing with the emission, and the above-mentioned displacement of the electronic states in the CB bottom and VB top. These effects influence the processes of excitation energy transfer to the luminescence centers, eventually leading to complicated dependence of the light output on the relative concentration of the substitutional cations.

One of the way to estimate an efficiency of excitation energy transfer to emission centers is a study of luminescence excitation spectra. The enhancement of intensity in the excitation spectrum in the energy region of separated

charge carriers creation indicates the increase of their probability to be transferred to the luminescence centers. Actually the efficiency of luminescence center excitation depends on a distance of their migration from each other and from the luminescence center, which will capture them. Therefore, the comparison of excitation spectra in the energy region of a separated e-h pairs creation ($E > E_g$) for compounds from one family allows to estimate a variation of charge carriers free path.

In the region above fundamental absorption edge an excitation of rare earth dopant luminescence centers can be realized via two channels. The first one follows the scheme (I): (e+h – «ex» – $RE^{3+(*)}$ – RE^{3+} + hv), the second one follows the scheme (II): RE^{3+}+ h / e – $RE^{4+/2+}$ + e / h – $RE^{3+(*)}$ – RE^{3+} + hv [17], where RE – rare-earth ion, «ex» – exciton. In the first case an electron and hole create an exciton, which is captured by the RE ion with subsequent emission of the luminescence quantum. In the excitation spectra usually an excitonic peak is observed in the region of a fundamental absorption edge which is followed by the subsequent gradual decrease of emission intensity at higher energies up to the edge of photon multiplication process [17]. In the second case the RE^{3+} is excited by a consecutive capture of a hole/electron and then of an electron/hole, that in some cases leads to a gradual increase of intensity in the excitation spectrum at $E > E_g$.

An analysis of excitation spectra allows to identify, which scheme is realized in the energy transfer to the emission centers or even determine the origin of the centers. For instance, an intrinsic emission is excited starting from a fundamental absorption edge, whereas a defect related emission can be excited in the transparency region of crystal as well.

In order to study the impact of the mentioned effects on the processes of energy transfer to the luminescence centers and consequently on the light output, the solid solutions of complex oxides with the substitutional cations of Y and Lu were chosen. The choice of these elements (both are from the family of rare earth metals) ensures similarity of their chemical properties and ionic charge, which is of paramount importance for creating single-phase solutions.

2. SOLID SOLUTIONS

Tuning chemical composition of substitutional solid solutions is one of efficient ways to engineer new materials with the required and specified properties. A substitutional solid solution is a crystalline phase of variable composition, in which substitutional cations occupy equivalent positions in a common crystal lattice. For the successful formation of solid solutions the following Goldschmidt rules should be fulfilled: i) the ionic radii of substitutional cations should differ by no more than 15% and ii) their charges may differ by unity when an electroneutrality is achieved by pairwise substitution. Also the Vegard's law should be fulfilled. According to this empirical statement the lattice parameters of a solid solution should vary linearly with gradual substitution of components in the solid solution [18] in the whole range of their concentrations.

An advantage of solid solutions is an opportunity to change the physical, mechanical, or electronic properties in comparison to the constituting "pure" components, when only one kind of cation from the considered pair is present in the crystal lattice (like $Zn_xMg_{1-x}WO_4$ solution and $ZnWO_4$, $MgWO_4$ "pure" components). The modifications of physical properties are determined primarily by the superstructure, which is formed during the synthesis process by transition from the high temperature state to the low temperature state of a solid solution [19]. The high-temperature state is a homogeneous solid solution, in which the substitutional atoms are randomly distributed in the lattice sites. Such state is disordered. With the decrease of temperature a phase transformation occurs, during which the crystal lattice of a disordered solution divides into several non-equivalent sub-lattices. Each of these sub-lattices forms an ordered phase. Thus, the phase transformation is a result of redistribution of crystal lattice ions between different sub-lattices. If the redistribution occurs on the scale comparable with the interatomic distances, then the ordered phase is formed. If, however, the redistribution occurs on the scale, which is significantly larger than the interatomic distance, then the homogeneous solid solution is divided into several ordered phases. It is the so-called short-range order in a solid solution. The ordered phases form clusters with different composition. If the size of such clusters is larger than the lattice constants, they can be detected as individual peaks in the diffraction pattern. If, on the contrary, these clusters are smaller than several lattice constants, they can be detected only by the Raman scattering or small-angle X-rays or neutrons scattering [20].

Currently, the metals solid solutions (alloys) were studied in great details. The short-range order in crystalline alloys occurs in a certain temperature range and leads to the changes of physical and mechanical properties [21]. For example, in the $Cr_{20}Ni_{80}$ alloy (nichrome) an anomalous increase of electrical resistance and changes in strength properties were detected. Moreover, the effect of the electrical resistance increase occurs in the case of the short-range

order and is explained by dependence of an electron free path length on the alloy components concentration.

It is expected that the similar effect of modification of the electron free path length can be observed in crystalline substitutional solid solutions (or mixed crystals). It was proposed that for some compounds this effect results in the increase of luminescence intensity for an intermediate concentration of substitutional cations, which is usually defined by the **x** value (with **x** typically varying in the range from 0 to 1). For instance, this effect was detected in several sets of solid solutions, such as perovskites $Lu_xY_{1-x}AlO_3$:Ce [7], borates $Lu_{1-x}Sc_xBO_3$:Ce [10], silicates $(Lu,Gd)_2SiO_5$:Ce [9], garnets $Y_3(Al_{1-x}Ga_x)_5O_{12}$:Ce [8], tungstates $Zn_xMg_{1-x}WO_4$ [13]. The increase of luminescence intensity does not depend on a type of crystal structure, and it is observed in the cases of both cationic and anionic solid solutions [15]. Several hypotheses were suggested to explain the physical origin of supposed limitation of distance between the charge carriers in the mixed crystals.

For example, it was proposed [16] that the observed enhanced luminescence is due to increasing number of phonon branches in solid solutions. However, the proposed increase of the phonon modes number does not play a significant role if a solid solution has many atoms in the unit cell (e.g. in ternary oxides).

Another explanation was offered in ref. [15]. The clusterization as a result of the short-range order is proposed similarly to the case of metal alloys [19]. The clusters boundaries create a potential barrier for the separated e and h, which are formed after absorption of the excitation photons. The barrier decreases the probability for charge carriers to cross over the cluster boundaries and results in the decrease of the average distance between the charge carriers. Finally, the probability of their localization on the same emission center increases with subsequent light output enhancement.

Variation of the electronic structure of a solid solution in comparison to its constituents is also considered as one of the reasons of the distance limitation between already thermalized e and h. If the CB bottom and/or the VB top are mainly formed by the states of substitutional cations, the localization of thermalized charge carriers in the spatial fluctuations of energy wells at the CB bottom and/or VB top are possible [16]. It is noted that the radiative recombination of charge carriers is effective only if the distance between the genetic e-h pairs is comparable with the Onsager radius [15].

3. AIM OF THE STUDY

The main goal of the thesis was to determine the influence of the electronic structure and phase composition of the mixed crystals as well as the limitation of charge carriers free path on the luminescent properties and the processes of energy transfer to the luminescence centers in the mixed crystals of $Lu_xY_{1-x}BO_3$, $Lu_xY_{1-x}PO_4$, and $Lu_xY_{1-x}VO_4$, undoped and doped with Eu^{3+} or Ce^{3+}. To achieve this, the following specific objectives were pursued:

1) synthesis of the borates, phosphates, and vanadates solid solutions, undoped and doped with Ce^{3+} or Eu^{3+}, and study of the influence of annealing procedure on the solid solutions formation;
2) study of the crystal structure and phase composition of the solid solutions in relation to the relative concentrations of the substitutional cations by X-ray diffraction (XRD) and Raman spectroscopy;
3) study the energy transfer processes from the host to intrinsic and dopant luminescence centers in a wide temperature range by luminescence spectroscopy in the UV-VUV and X-ray energy ranges;
4) study of the bandgap modification with the concentration of substitutional cations by an analysis of the thermally stimulated luminescence (TSL) curves.

4. EXPERIMENTAL

4.1. Synthesis of the materials

The $Lu_xY_{1-x}PO_4$ solid solutions, undoped (**x** = 0, 0.5, 1) and doped with 0.5 mol % Ce^{3+} or 0.5 mol % Eu^{3+} (**x** = 0, 0.1, 0.3, 0.5, 0.7, 0.9, 1.0), and the $Lu_xY_{1-x}BO_3$ solid solutions, undoped (**x** = 0, 0.65, 1) and doped with 1 mol % Ce^{3+} or 1 mol % Eu^{3+} (**x** = 0, 0.25, 0.5, 0.75 1.0), were synthesized by the sol-gel method and provided by Dr. B.I. Zadneprovski (Central Research and Development Institute of Chemistry and Mechanics, Moscow, Russia).

Synthesis of the vanadate $Lu_xY_{1-x}VO_4$ mixed crystals (**x** = 0, 0.1, 0.3, 0.5, 0.7, 0.9, 1), undoped and doped with 1 mol % of Eu^{3+}, was carried out by the solid state reaction method. For the synthesis, the reagent-grade starting materials Lu_2O_3 (Stanford Materials Corporation, 99.995%), Y_2O_3 (Stanford Materials Corporation, 99.999%), Eu_2O_3 (Stanford Materials Corporation, 99.999%) and V_2O_5 (Riedel-de Haen, 99,5%) were used. The boric acid H_3BO_3 (Carl Roth GmBH + Co, 99.8%) was used as the catalyst to reduce the melting point and ensure better mixing of the reagents. The reagent-grade starting materials were thoroughly mixed and ground in an agate mortar. Then the mixtures were air heat-treated in alumina crucibles consequently in several steps. The first annealing was carried out at 1000 ^oC for 2 hours in air followed by natural cooling down to the room temperature. Then, the grinding of obtained powders was produced in an agate mortar with addition of boric acid one more time, and this procedure was repeated once at 1000 ^oC and one more time at 1200 ^oC. The temperature increase up to 1200 ^oC is connected with the features of crystallization of solid solutions. The crystal structure was checked after every step of annealing procedure. As a result, the $Lu_xY_{1-x}VO_4$ solid solutions (**x** = 0, 0.1, 0.3, 0.5, 0.7, 0.9, 1), both undoped and doped with 1 mol % Eu^{3+}, were synthesized. In all compounds **x** value is the relative concentration of Lu ions, **1-x** value is the relative concentration of Y ions.

4.2. Experimental techniques

In this section the experimental techniques used for characterization of the samples and the studies of luminescence properties are described. The crystal structures were determined by using the powder X-ray diffraction analysis. The XRD method is one of the most prevalent methods for analysis of the crystal structure type and the phase composition; it also allows to evaluate the lattice parameters and the crystallite size of a powder. The Raman spectroscopy was used for the analysis of the crystal structure type as an additional method for the structure control. The set-ups used for the measurements of luminescence spectra, luminescence excitation spectra, the temperature dependence of X-ray excited luminescence, the thermally stimulated luminescence curves and the kinetics of luminescence decay are described as well.

4.2.1. X-Ray diffraction analysis

To monitor completeness of the reaction and phase purity of the final product, the XRD analysis of the borate and phosphate solid solutions were carried out using a Rigaku Ultima IV X-ray diffractometer.

The crystal structure of vanadate solid solutions were studied by a Bruker D8 Advance Diffractometer. The measurements were performed in the full range of $2\theta = 10\text{-}80°$ with $2\theta = 0.032°$ step and in short range $2\theta = 23\text{-}27°$ with $2\theta = 0.008°$ step at room temperature. The latter range was measured with high angular resolution to resolve details of the solid solutions structure. Both diffractometers are equipped with a nickel-filtered Cu $Ka_{\alpha 1}$ radiation source with $\lambda = 1.540596$ Å.

4.2.2. Scanning electron microscopy

The morphology of the phosphate solid solutions was determined by means of a Quanta 3D FEG Scanning Electron Microscope. The morphology of vanadate solid solutions was determined by a Hitachi S-3400 N Scanning Electron Microscope equipped with energy dispersive X-ray spectroscopy analyzer. The granulometric analysis was carried out using a laser diffraction analyzer Shimadzu SALD-2201.

4.2.3. Raman spectroscopy

Raman spectroscopy is a simple and qualitative method of chemical analysis of a material, its purity, spatial distribution of impurities, crystallinity and phase transitions. This method is applicable in a wide energy range from UV to the near infrared (IR), allowing to select the most convenient range for the studied sample. It is worth noting that the Raman spectroscopy is a non-destructive method in comparison to XRD method, and does not require a pre-treatment of the sample.

The Raman scattering spectra were measured in the back-scattering geometry at room temperature through 50× microscope objective using a Renishaw inVia micro-Raman spectrometer equipped with an argon laser (514.5 nm, power $P_{ex} = 0.1$ mW). The spectral signal was dispersed by 2400 gr/mm diffraction grating onto a Peltier-cooled CCD detector.

4.2.4. VUV spectroscopy with synchrotron radiation

The YPO_4 and $LuPO_4$ phosphates are insulators with the bandgap exceeding 8.5 eV. To excite the intrinsic luminescence in such wide-gap compounds, VUV excitation sources should be used. The synchrotron radiation (SR) is the most convenient excitation source for the study of the luminescent properties of

wide-gap materials due to its high intensity continuous radiation in a wide spectral range from IR to X-ray, and its time structure as well [22].

The luminescence and excitation spectra, luminescence decay kinetics of borates and phosphates under excitation in the energy range from 3.7 to 22 eV were measured at the SUPERLUMI experimental station using SR (DESY, Hamburg, Germany) [23]. The samples were placed in a helium flow optical cryostat providing measurements over a wide temperature range from 4.2 to 400 K. The time-resolved luminescence spectra were recorded in the time windows from 5 to 20 ns and from 80 to 100 ns with respect to the maximum of the SR excitation pulse. The time windows were chosen to separate the "fast" (intracenter transitions or energy transfer from excitons to Ce^{3+}) and "slow" (energy transfer of spatially separated electron-hole pairs to the Ce^{3+} centers) processes of energy transfer to Ce^{3+} ions.

4.2.5. UV and visible luminescence spectroscopy

Laboratory setup at Moscow State University (Russia)

The luminescence and luminescence excitation spectra were measured in the UV and visible ranges on a set up based on the LOT-Oriel MS-257 spectrograph at the Department of Physical Problems of Quantum Electronics of the Skobeltsyn Institute of Nuclear Physics, M.V. Lomonosov Moscow State University (Russia). This setup allows to carry out the measurements of luminescence spectra in the range of 200-1050 nm and luminescence excitation spectra in the range of 200-500 nm at temperatures in the range of 80-500 K. The luminescence spectra were normalized to the instrumental sensitivity function.

Laboratory setup at University of Tartu (Estonia)

Experiments in the energy range 2.5-8 eV were carried out on the VUV laboratory setup for luminescence spectroscopy of the Institute of Physics, University of Tartu. A deuterium D 200 VUV lamp has been used as the excitation source. The excitation wavelength was selected using a primary monochromator McPherson Model 234/302. The samples were mounted into an optical vacuum cryostat, which allows to perform measurements in the temperature range 5-300 K. A Shamrock 303i (Andor Technology) was used as a secondary monochromator. The luminescence was detected using a Hamamatsu H8259 photon counting head.

Laboratory setup at Institute of Physics, Czech Academy of Science in Prague (Czech Republic)

The temperature dependence of photoluminescence spectra of the undoped vanadates were measured on the laboratory setup at Institute of Physics, Czech Academy of Science in Prague. The custom made a 5000M Horiba Jobin Yvon fluorescence spectrometer was used in the experiments. A liquid nitrogen bath optical cryostat (Janis) was used in the temperature dependence measurements

(77-500 K). The photoluminescence of the samples was excited by a deuterium lamp (Heraus Gmbh).

4.2.6. Luminescence spectroscopy with X-ray source

Laboratory setups with X-ray source (Lyon, France)

The measurements of the X-ray luminescence, TSL curves and their spectral composition for the phosphates and vanadates were carried out at the Institute of Light and Matter, University of Claude Bernard Lyon 1 (Lyon, France). The measurements of luminescence spectra were carried out under irradiation with X-rays generated by tube INEL XRG 3000 with a tungsten anode operating at 30 keV and 20 mA. The spectra were registered using a Shamrock 500i spectrograph equipped with Newton EMCCD DU970P. The luminescence spectra were recorded in the temperature range 80-550 K. All spectra were corrected for the setup spectral distortions.

The TSL curves were detected using a Shamrock 500i spectrometer with an ANDOR Newton CCD camera. The samples were mounted into a LINKAM THMS600 Stage, which allowed to perform TSL measurements in the temperature range 80-450 K with linear heating rate 0.167 K/s.

The decay curves of doped Ce^{3+} phosphates were measured with a pulsed X-ray source. The source consists of the light-excited X-ray tube Hamamatsu N5084 and the laser diode. When the light from the laser diode is absorbed by the photocathode the electrons are released. The released electrons are accelerated by the potential 30 kV to anode, where X-rays are produced upon impact. The luminescence of samples is excited by these pulsed X-rays. The luminescence signal is registered using Photomultiplier Detector Assembly PMA 182 with timing resolution < 180 ps (FWHM) and processed by Standalone TCSPC Module with USB Interface PicoHarp 300.

Laboratory setup with X-ray source (Wroclaw, Poland)

The measurements of X-ray excited luminescence of vanadate solid solutions were carried out at the Faculty of Chemistry, University of Wroclaw (Poland). The X-ray excited luminescence spectra were recorded using a radiation from a Cu X-ray tube operating under the voltage of 40 kV and the current of 10 mA. The emission photons were collected using 74-UV lens connected to a QP600-2-SR-BX waveguide, which transfers the luminescent light to an Ocean Optics HR2000CG-UV-NIR Spectrometer.

4.2.7. Luminescence spectroscopy with electron gun

TSL measurements of the phosphate solid solutions doped with Ce^{3+} were also performed in the laboratory of ionic crystals at the Institute of Physics, University of Tartu (Estonia). The TSL curves were detected on the experimental

setup with an electron gun (5 keV, 0.4μA, spot≈1mm^2) as the irradiation source in the temperature range 80-400 K with a linear heating rate 0.167 K/s. All measurements were carried out in a liquid helium vacuum cryostat (5-400 K temperature range, 2*10^{-7} Torr) equipped with LakeShore 331 Temperature Controller. The TSL curves were detected using the UV-VIS-NIR (200-1700 nm) monochromator (ARC SpectraPro-2300i) with a Hamamatsu photon counting head H6240 detector.

4.2.8. Fitting (approximation) of TSL curves

A fitting of all TSL curves were carried out using the first order decay approximation assuming that the VB top and CB bottom have a flat structure. This approximation supposes that free charge carriers more likely form excitons, than are recaptured by traps. An elementary peak in such approximation is described by equation (1):

$$I_{lum} = n(0)\omega_0 \exp\left(-\frac{E_A}{\kappa_B T(t)} - \frac{\omega_0 \kappa_B T^2(t)}{E_A T'(t)} \exp\left(-E_A / \kappa_B T(t)\right)\right), \quad (1)$$

where *n(0)* – the traps concentration, ω_0 – the frequency factor, E_A – the activation energy, *T(t)* – the sample temperature, *T'(t)* – the heating rate [17]. In all experiments the heating rate was constant *T'(t)*=10 K/min.

This approximation does not take into account interactions between different types of traps. A profile of TSL peak can be satisfactorily fitted by only one set of parameters including the activation energy of traps E_A.

5. RESULTS AND DISCUSSION

5.1. Vanadate solid solutions

In this section the detailed study of the luminescent and structural properties of the $Lu_xY_{1-x}VO_4$ solid solutions, both undoped and doped with Eu^{3+} ions, depending on the synthesis conditions and the relative concentration of substitutional cations, is presented. In particular, the main attention was focused on the study of the energy transfer processes from the host to the intrinsic and impurity luminescence centers.

5.1.1. XRD study of $Lu_xY_{1-x}VO_4$ solid solutions

The crystal structure and phase composition after every step of the annealing procedure were controlled by the XRD method (section 4.2.1) in order to optimize the temperature and time of calcination of the samples. As a result, certain changes in the positions and shapes of the XRD lines were detected. The XRD lines shift towards increasing 2θ angle with the increase of Lu^{3+} concentration in the $Lu_xY_{1-x}VO_4$:Eu^{3+} samples. The shift of XRD lines can be explained by a decrease of the unit cell size with gradual substitution of Y^{3+} (ionic radius 1.019 Å) with smaller Lu^{3+} (ionic radius 0.977 Å). The gradual shift of the X-ray diffraction line in the range of 2θ = ~25° with increase of the **x** value is clearly observed in fig. 1. The decrease of intensity and the broadening of this diffraction peak was registered and it was the most pronounced feature for the crystal with **x** = 0.5. After first calcination at 1000 ºC the XRD line demonstrates a doublet structure for the intermediate **x** values (fig. 1a). The non-elementary structure of XRD line indicates an irregular distribution of the substitutional cations Y and Lu. As a result, agglomerations of the yttrium or lutetium vanadate in different areas of a crystallite are formed.

After further annealing steps the distribution of the substitutional cations becomes more homogeneous. The XRD line becomes a singlet, narrower and more symmetrical (fig. 1b). Nevertheless, certain broadening of this line is observed for the solid solutions in comparison to their constituents. This effect can be associated with a distortion of the unit cell due to the difference of ionic radii of Lu^{3+} and Y^{3+}, which forms the local irregular deformations in the crystal lattice.

Using original experimental XRD data, the calculations of the lattice constants **a** and **c** for $Lu_xY_{1-x}VO_4$ were carried out. Additionally, the lattice constants were calculated using the empirical model presented in ref [24]. The change of **a** and **c** follows the Vegards' law and can be fitted to the linear function. All calculated values are in good agreement with the experimental ones (see table 1).

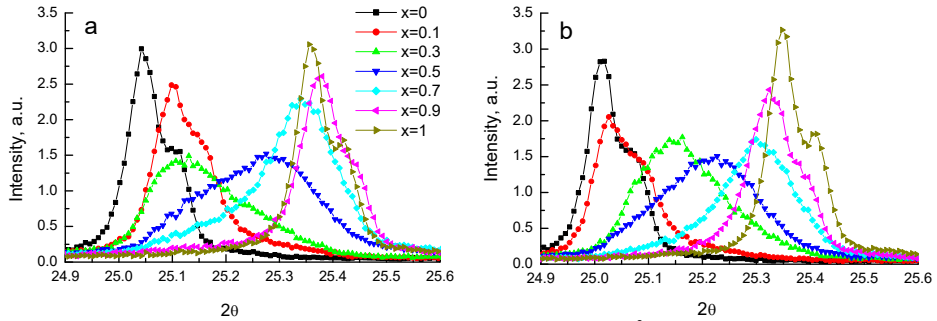

Figure 1. The X-ray diffraction pattern of $Lu_xY_{1-x}VO_4:Eu^{3+}$ in the range of 2θ = ~25° after annealing at 1000 °C (a) and at 1000 °C, 1000 °C, 1200 °C (b).

Table 1. Lattice parameters (all in Å) of the $Lu_xY_{1-x}VO_4$ solid solutions derived from the experimental XRD data and calculated using the empirical model [24].

	Experiment, XRD		Empirical model	
Sample	*a*	*c*	*a*	*c*
YVO_4	7.107	6.303	7.1118	6.2911
YVO_4:Eu	7.116	6.299	7.1128	6.2918
$Lu_{0.1}Y_{0.9}VO_4$	7.080	6.283	7.1023	6.2853
$Lu_{0.1}Y_{0.9}VO_4$:Eu	7.116	6.287	7.1032	6.2860
$Lu_{0.3}Y_{0.7}VO_4$	7.080	6.282	7.0830	6.2737
$Lu_{0.3}Y_{0.7}VO_4$:Eu	7.080	6.293	7.0841	6.2744
$Lu_{0.5}Y_{0.5}VO_4$	7.062	6.269	7.0638	6.2621
$Lu_{0.5}Y_{0.5}VO_4$:Eu	7.062	6.280	7.0649	6.2977
$Lu_{0.7}Y_{0.3}VO_4$	7.045	6.244	7.0447	6.2504
$Lu_{0.7}Y_{0.3}VO_4$:Eu	7.036	6.248	7.0457	6.2511
$Lu_{0.9}Y_{0.1}VO_4$	7.018	6.246	7.0255	6.2388
$Lu_{0.9}Y_{0.1}VO_4$:Eu	7.036	6.237	7.0265	6.2395
$LuVO_4$	7.027	6.231	7.0159	6.2330
$LuVO_4$:Eu	7.028	6.242	7.0179	6.2343

5.1.2. Luminescence origin and its intensity dependence on x in vanadate solid solutions

The luminescence spectra of $Lu_xY_{1-x}VO_4$, both undoped and doped with Eu^{3+} under X-ray excitation are presented in fig. 2 and fig. 3. The peaks at around 460 nm are associated with the intrinsic emission of the vanadates and originates from the self-trapped excitons (STE) emission [25-27] or charge-transfer transitions within the $(VO_4)^{3-}$ complexes [28-29]. The luminescence band gradually shifts to longer wavelengths from 450 nm in YVO_4 up to 470 nm in $LuVO_4$ (fig.2). The substitutional cations do not form the emission centers, however, they change the value of crystal field that influences the position of energy levels of $(VO_4)^{3-}$ emission centers.

In the $Lu_xY_{1-x}VO_4:Eu^{3+}$ only the dopant emission is observed at 300 K, which originates from 4f-4f intraconfigurational transitions in Eu^{3+} ions, while the intrinsic emission is completely quenched [27]. At lower temperatures both intrinsic and dopant emissions were observed (fig. 3b).

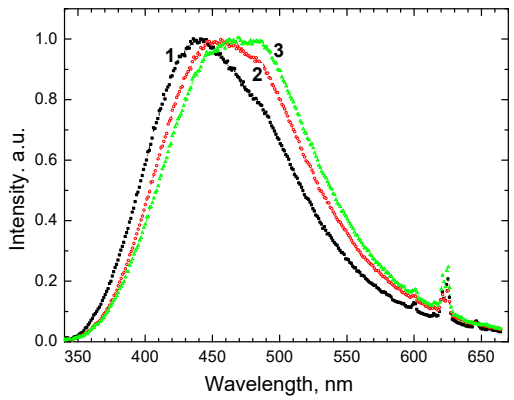

Figure 2. The luminescence spectra of the undoped $Lu_xY_{1-x}VO_4$ for **x** = 0 (1), **x** = 0.5 (2) and **x** = 1 (3) under X-ray excitation at T = 300 K.

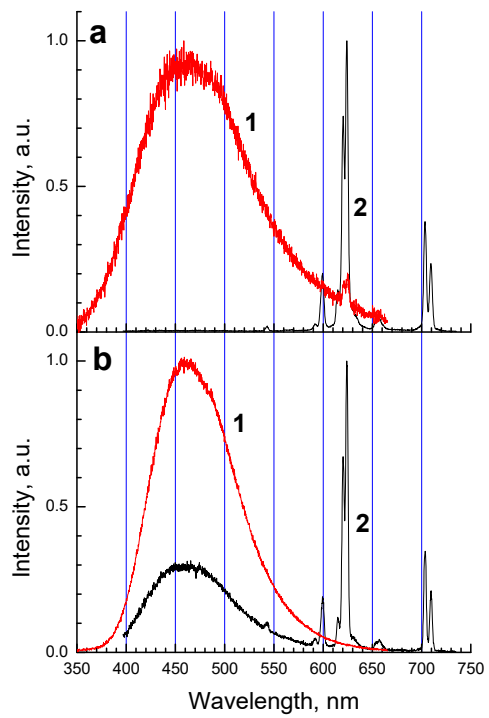

Figure 3. The luminescence spectra of the undoped (1) and doped with Eu^{3+} (2) $Lu_{0.5}Y_{0.5}VO_4$ under X-ray excitation at T = 300 K (a) and 85 K (b).

The intensity of X-ray excited luminescence was studied after each step of the annealing procedure (fig. 4). The increase of the luminescence intensity was observed for all sets of the solid solutions obtained after each subsequent annealing. The intensity increase after each annealing could be associated with the enhancement of the solid solutions crystallinity that was confirmed by the XRD data (section 5.1.1) and with the increase of the particles size that was observed by SEM (see publication I). After the third step of annealing (1000 °C, 1000 °C, 1200 °C) the maximal luminescence intensity was observed for the undoped $Lu_xY_{1-x}VO_4$ with **x** = 0.7 and for the $Lu_xY_{1-x}VO_4:Eu^{3+}$ with **x** = 0.3 and **x** = 0.7 (fig. 4b).

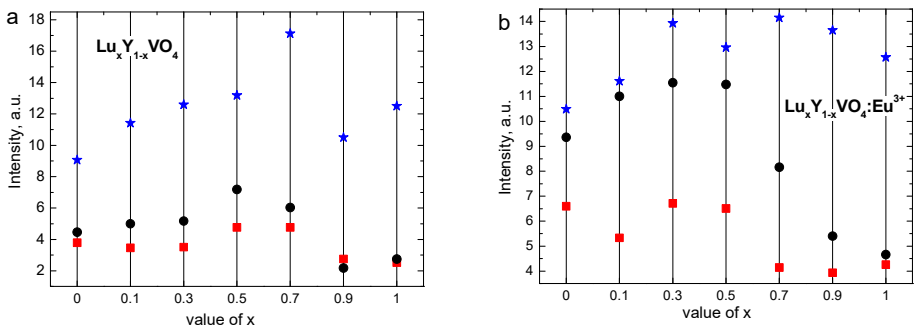

Figure 4. The dependence of relative intensity of X-ray excited luminescence on the **x** value in $Lu_xY_{1-x}VO_4$, undoped (a) and doped with Eu^{3+} (b), after subsequent annealing at 1000 °C (squares), at 1000 °C, 1000 °C (circles), and at 1000 °C, 1000 °C, 1200 °C (stars), T = 300 K. In each point the intensity was obtained by integrating the spectrum in the region 350-730 nm for $Lu_xY_{1-x}VO_4$ and 500-750 nm for $Lu_xY_{1-x}VO_4:Eu^{3+}$.

5.1.3. Temperature dependence of vanadates luminescence

The analysis of temperature dependence of the luminescence intensity under both X-ray and photo- excitation of the undoped $Lu_xY_{1-x}VO_4$ shows that the intrinsic emission is substantially quenched at 300 K (fig. 5). The quenching temperature of luminescence depends on the **x** value, herewith the samples with intermediate **x** value have a higher quenching temperature. The inset of fig. 5a shows the dependence of quenching temperature on the **x** value, where the quenching temperature is determined by the decrease of intensity by factor of 2 relatively to that at 85 K. Thus, the maximum luminescence intensity of $Lu_xY_{1-x}VO_4$ with **x** = 0.7 at 300 K is associated with the higher luminescence quenching temperature for this sample.

It is worth noting that the intrinsic emission of $Lu_xY_{1-x}VO_4:Eu^{3+}$ is completely quenched at 300 K, in comparison to the undoped vanadates. It is due to efficient energy transfer from the host to the dopant emission centers. Moreover, the effect of temperature quenching does not influence the Eu^{3+} luminescence intensity at 300 K.

The temperature dependence of intrinsic and dopant emission in the $Lu_xY_{1-x}VO_4:Eu^{3+}$ solid solutions are shown in fig. 6. The dependencies have an antibate behavior at T = 80-200 K that indicates the competing process of energy relaxation between the STE and Eu^{3+} emission centers. At low temperatures the localization of excited charge carriers at VO_4^{3-} groups is most probable that reduces the probability of their migration to the Eu^{3+} ions. It can be due to a self-trapping of one type of charge carriers (presumably, holes) at VO_4^{3-} groups that prevents the energy transfer to the dopant ions. With the increase of temperature the energy of lattice vibrations becomes sufficient for the thermal release of self-trapped charge carriers. It allows their migration to long distances and increases the probability of their capture by the dopant. The release of charge carriers from traps usually is followed by an appearance of TSL peaks. Indeed, for the vanadate solid solutions several TSL peaks were detected in the temperature range 100-200 K (fig.7).

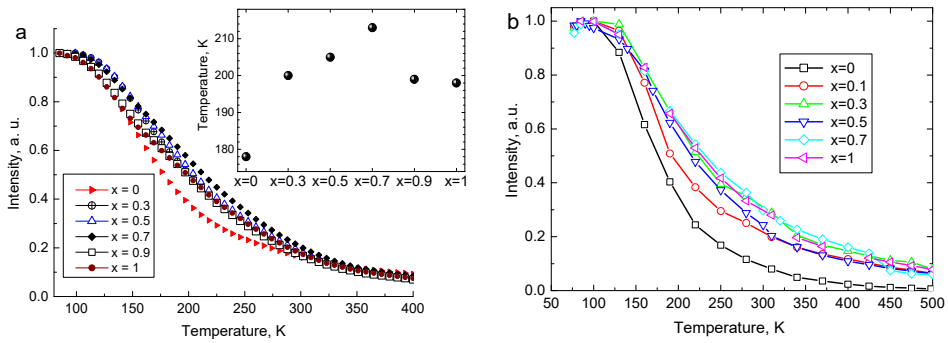

Figure 5. The temperature dependence of luminescence intensity under X-ray (a) and photo- (b) excitation (E_{ex} = 4.1 eV) of the undoped $Lu_xY_{1-x}VO_4$ solid solutions. The inset shows the dependence of quenching temperature on **x** value.

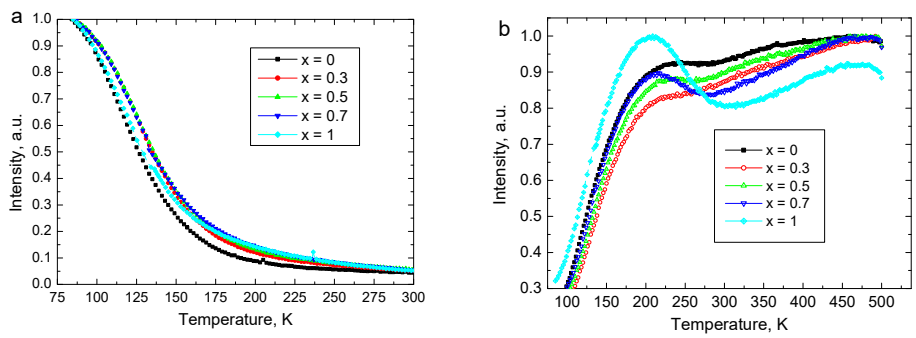

Figure 6. The temperature dependence of STE (a) and Eu^{3+} emission (b) in $Lu_xY_{1-x}VO_4:Eu^{3+}$ under X-ray excitation.

5.1.4. Thermally stimulated luminescence of vanadate solid solutions

The influence of **x** value in $Lu_xY_{1-x}VO_4$ on their structural defects was studied using the TSL method. The TSL curves of undoped $Lu_xY_{1-x}VO_4$ are shown in fig. 7. The curves consist of several overlapping peaks in the temperature range 80-230 K. The peaks at 110 K (1), 160 K (2), and 180 K (3) were detected in all samples. With the increase of **x** value the shape of curves slightly changes that is caused by the redistribution of the intensity of TSL peaks. However, the peaks do not shift with **x** value.

The luminescence spectra of the TSL peaks of $Lu_xY_{1-x}VO_4:Eu^{3+}$ consist of both STE emission and Eu^{3+} emission as in the case of steady luminescence. The TSL curves measured in the emission band of STE and Eu^{3+} are presented in fig. 8a and b, respectively. The structure of the curves is similar to that of the undoped vanadates. The main difference is the appearance of the additional peak at 245 K.

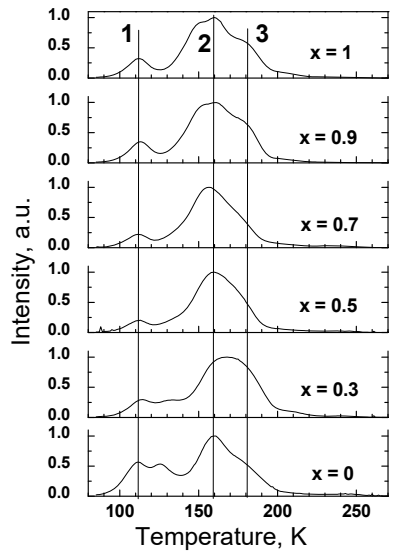

Figure 7. The TSL curves of the undoped $Lu_xY_{1-x}VO_4$ solid solutions measured in the emission band of STE.

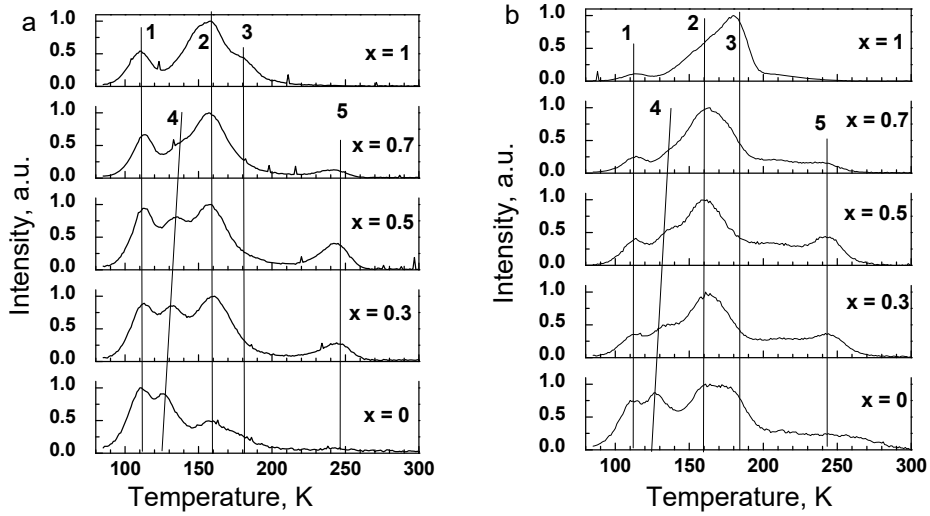

Figure 8. The TSL curves of the $Lu_xY_{1-x}VO_4:Eu^{3+}$ solid solutions measured in the emission band of STE (a) and Eu^{3+} emission (b).

Even slight changes in the activation energy of traps (a few tens of meV) can be detected by the shift of TSL peak position. The changes of traps depth usually allow to trace the bandgap modification associated with the shift of the CB bottom or the VB top (see more details in section 5.2.4 and publication II). However, in the vanadates solid solutions, both undoped and doped with Eu^{3+}, the position of TSL peaks 1-3 does not change. This result indicates the absence of the bandgap modification. Moreover, it correlates with the absence of the shift of fundamental absorption edge with change of the **x** value deduced from the analysis of luminescence excitation spectra (see section 5.1.5). However, the assumption of absence of the bandgap modification contradicts to the following results. The STE emission band shifts with the **x** value change (see section 5.1.2). The Raman spectra analysis also shows a gradual increase of the frequencies of the internal modes of VO_4^{3-} complexes with the increase of the **x** value (see publication I). It is worth noting that the CB bottom and VB top are formed mainly by the electronic states of the VO_4^{3-} complex, and the changes of the states of this complex produce strong impact on the energy structure of the whole matrix. Therefore, in both cases the observed modifications indicate the crystal field strength change and its influence on the VO_4^{3-} complexes and, as result, on the band structure of vanadates solid solutions.

To avoid the contradiction between the obtained results we suppose that the most intensive TSL peaks 1-3 correspond to a release of one type of charge carriers from the traps (electron or hole traps). An exception is the TSL peak at 120-130 K, which is clearly observed only for low values of **x** (**x** = 0; 0.1; 0.3; 0.5). Its maximum shifts to higher temperatures with the increase of **x** value. Therefore, this peak corresponds to the release of another type of charge carriers

in comparison to other TSL peaks and indicates the modification of the bandgap. In the case of vanadates we cannot definitely ascribe the type of traps (hole or electron), because the europium ion is not a stable electron trapping center in the vanadates [31].

The weak influence of the **x** value on the bandgap modification may be due to the fact that the VB top is formed mainly by the O 2p states, and CB bottom – by the V 3d states. The change of Lu/Y ratio results in the modification of density of electronic states in the depth of CB and VB and does not considerably influence the formation of the bandgap value [30].

5.1.5. Luminescence excitation spectra of vanadate solid solutions

The luminescence excitation spectra of undoped $Lu_xY_{1-x}VO_4$ are presented in fig. 9. The luminescence is excited starting from the fundamental absorption edge that is characteristic of the intrinsic emission. The onset of the excitation spectra at 3.5-3.6 eV allows to estimate the bandgap value of the $Lu_xY_{1-x}VO_4$ solid solutions. The obtained value of E_g is in good agreement with the literature data [30, 32-33]. It is worth noting that there is no noticeable shift of the onset with the **x** value that indicates a slight change of the bandgap, if any.

The excitation spectra of $Lu_xY_{1-x}VO_4$ and $Lu_xY_{1-x}VO_4:Eu^{3+}$ were normalized to unity in the first excitation peak at 3.8 eV, which is associated with the direct creation of excitons. At higher energies the luminescence excitation occurs as a result of the creation of separated electron-hole pairs, which may be bound into excitons after the thermalization and migration stages of energy relaxation. The luminescence intensity in the excitation spectra depends on the **x** value in this energy range and it increases for the intermediate **x** values. It demonstrates that the efficiency of energy transfer from the host to the emission centers (STE or Eu^{3+}) increases at intermediate **x** values. It is maximal for **x** = 0.3, 0.7, and 0.5, i.e. for the samples, which demonstrate maximal luminescence intensity under X-ray excitation (fig.4) and, therefore, can be connected with the enhancement of the energy transfer efficiency to the emission centers. The origin of the effect can be explained by the limitation of charge carriers free path in the solid solution (see introduction, ref [16, 18], and publication I). As a result, a probability of their capture by the same Eu^{3+} ions increases. It is worth noting that while in case of the undoped vanadates this effect plays a minor role, in the Eu^{3+} doped samples it is the main effect, which determines the formation of luminescence intensity dependence on the **x** value.

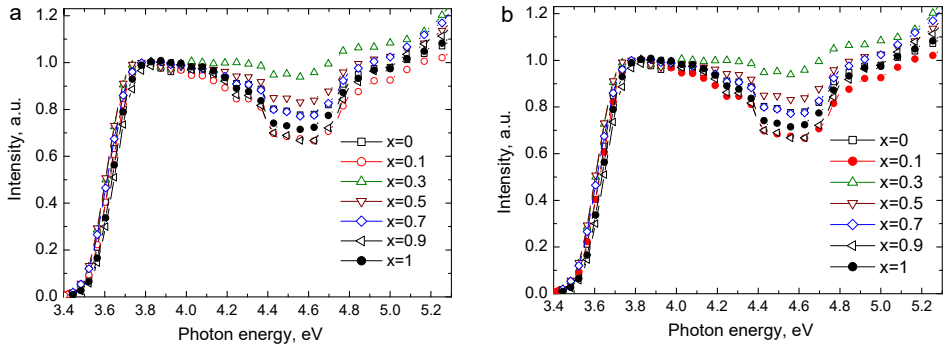

Figure 9. The photoluminescence excitation spectra of $Lu_xY_{1-x}VO_4$ (a), λ_{em}=450 nm and $Lu_xY_{1-x}VO_4:Eu^{3+}$ (b), λ_{em}=615 nm, T=300 K.

5.2. Phosphate solid solutions

In this section a detailed study of the luminescence properties of the $Lu_xY_{1-x}PO_4$ solid solutions, both undoped and doped with Ce^{3+} or Eu^{3+} ions is presented. All samples have the same crystal phase of xenotime, $I4_1/amd$ space group. It allows to exclude the impact of the several crystal phases on the energy transfer processes in crystals (as it will be shown below, for the borates the presence of additional phase considerably influence the energy transfer). Another feature of the studied phosphates is the absence of intrinsic emission at temperatures down to 5 K.

5.2.1. Luminescence properties of undoped $Lu_xY_{1-x}PO_4$

The luminescence spectra of undoped YPO_4, $Lu_{0.5}Y_{0.5}PO_4$, and $LuPO_4$ are presented in fig. 10. At least two overlapping luminescence bands peaking at 365 nm and 415 nm were observed under excitation at $E_{ex.}$=11 eV. The shape and position of the emission bands in YPO_4 and $Lu_{0.5}Y_{0.5}PO_4$ coincide, while for $LuPO_4$ the redistribution of the intensity of these bands was detected.

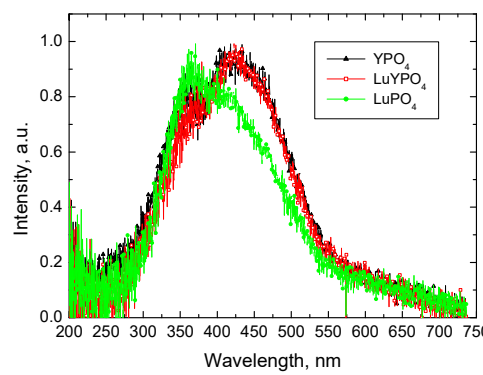

Figure 10. The luminescence spectra of YPO_4, $Lu_{0.5}Y_{0.5}PO_4$ and $LuPO_4$, $E_{ex.}$=11 eV, T=7 K.

Under selective excitation by E_{ex} = 11 eV, 7.8 eV, and 6 eV up to three luminescence bands were detected in UV- and blue spectral range (fig. 11, inset). The excitation spectra of these luminescence bands significantly vary that is connected with a different origin of the emission centers. Nevertheless, the common feature of these spectra is a rapid drop of the intensity at E_{ex} ~ 9 eV. This energy corresponds to the fundamental absorption edge because the bandgap in the studied phosphates is 8.8-9.2 eV [34-36]. Under excitation in the energy region below the fundamental absorption edge only the emission centers related to the defects of crystal structure can be excited in the undoped phosphates. An intrinsic emission is usually excited starting from the fundamental absorption edge. In the case of YPO_4, $Lu_{0.5}Y_{0.5}PO_4$, and $LuPO_4$ the intrinsic emission with characteristic excitation spectrum was not observed down to the low temperature limit of measurements T = 5 K.

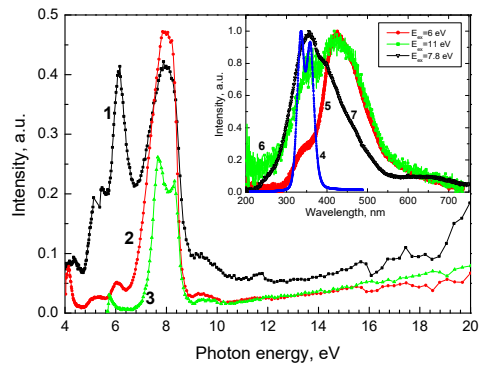

Figure 11. The luminescence excitation spectra of YPO_4 at $\lambda_{em.}$= 480 nm (curve 1), $\lambda_{em.}$= 325 nm (curve 2), and $\lambda_{em.}$= 250 nm (curve 3). The inset shows the luminescence spectra of $YPO_4:Ce^{3+}$ at E_{ex}=15.5 eV (curve 4) and YPO_4 at E_{ex} = 6 eV (curve 5), 11 eV (curve 6), and 7.8 eV (curve 7) T = 7 K.

Time-resolved luminescence excitation spectra

The time-resolved luminescence excitation spectra of the undoped phosphates are presented in fig. 12, inset. Such approach allowed to separate the "fast" and "slow" processes, which are responsible for the energy transfer to the defect related luminescence centers. The "fast" component of the excitation spectrum exhibits a complex structure in the transparency region of phosphate. The position of excitation bands is similar to those in the excitation spectra of the Ce^{3+} doped phosphates that indicates the contamination of nominally undoped sample by the Ce^{3+} impurities. The photoluminescence of $Lu_xY_{1-x}PO_4:Ce^{3+}$ consists of doublet in the range 310-390 nm (fig.11, inset), which overlaps with the luminescence spectrum of undoped phosphates.

The high-energy edge of broad excitation band with maximum at ~ 8 eV shifts by ~ 0.5 eV to high-energy region with the increase of **x** value (fig.12).

Such a shift follows the fundamental absorption edge and indicates the increase of the bandgap value from YPO_4 to $LuPO_4$.

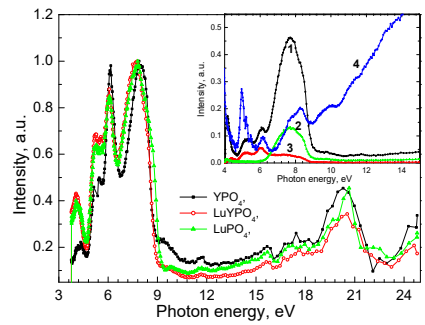

Figure 12. The luminescence excitation spectra of YPO_4, $Lu_{0.5}Y_{0.5}PO_4$, and $LuPO_4$ at λ_{em} = 450 nm, T = 7 K. The inset shows the integrated (curve 1), slow (curve 2), and fast (curve 3) components of the time-resolved excitation spectra of $Lu_{0.5}Y_{0.5}PO_4$ at $\lambda_{em.}$= 325 nm and excitation spectrum of $YPO_4:Ce^{3+}$ (curve 4) at $\lambda_{em.}$ = 365 nm, T=7 K. The "slow" processes were recorded in the time windows from 80 to 100 ns, the "fast" – from 5 to 20 ns.

5.2.2. Luminescence properties of $Lu_xY_{1-x}PO_4:Ce^{3+}$

The photoluminescence spectrum of $Lu_xY_{1-x}PO_4:Ce^{3+}$ at 300 K has a doublet structure with maxima at 330 and 355 nm, which are caused by the interconfigurational radiative transitions 5d - 4f ($^7F_{5/2,7/2}$) of the Ce^{3+} ions (fig. 13). The observed shift of the luminescence bands toward longer wavelength region with the increase of **x** value is associated with an increase of the crystal field strength due to the decrease of the lattice constants (see publication II). Under X-ray excitation an additional broad band was detected at 80 K, which is attributed to the emission of the host defects.

Temperature dependence of luminescence

The temperature dependence of X-ray excited luminescence of the $LuPO_4:Ce^{3+}$ and $YPO_4:Ce^{3+}$ samples in the range from 90 to 420 K are presented in fig. 14. The dependence of $YPO_4:Ce^{3+}$ demonstrates a plateau in the ranges 90-165 K and 210-330 K. The intensity increases by 20 % with the temperature increase from 165 to 210 K and decreases at T > 300 K that is connected with intracenter quenching with in Ce^{3+}. The quenching of the defect emission in $YPO_4:Ce^{3+}$ starts already from 100 K and at 300 K it is almost quenched. The thermal stability of the emission of the defects of $LuPO_4:Ce^{3+}$ and $YPO_4:Ce^{3+}$ differs, however in both cases the region of quenching does not correlate to the region of intensity rise of Ce^{3+} emission. Therefore, the processes of energy transfer from the host to these emission centers do not compete with each other. The observed rise of intensity for Ce^{3+} doped phosphates in the range 165-210 K

coincides with the position of TSL peaks (see section 5.2.4) and is connected with the thermal release of the charge carriers from the traps.

The relative luminescence intensity of Ce^{3+} doped solid solutions was studied (fig. 13, inset). For samples with **x** = 0.1 the most intensive emission was detected under UV- excitation, and the least intensive emission was observed for the solid solution with **x** = 0.5 under both UV- and X-ray excitations.

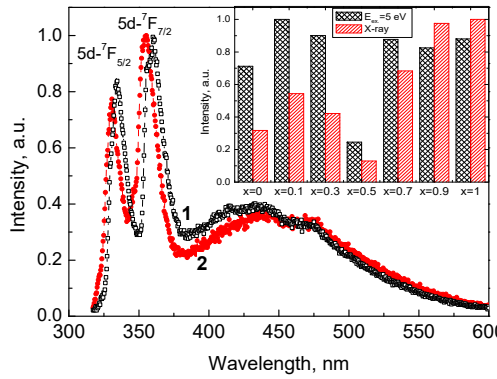

Figure 13. The luminescence spectra of $LuPO_4:Ce^{3+}$ (1) and $YPO_4:Ce^{3+}$ (2) under X-ray excitation, T=80 K. The inset shows the relative luminescence intensity of $Lu_xY_{1-x}PO_4:Ce^{3+}$ under UV ($E_{ex.}$ = 5 eV) and X-ray excitation, T=300 K.

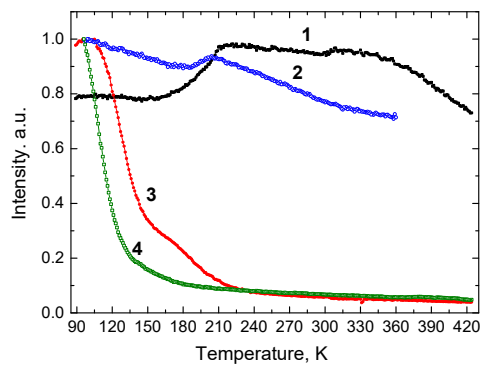

Figure 14. The temperature dependence of the Ce^{3+} (1,2) and defect (3,4) emission of $YPO_4:Ce^{3+}$ (1,3) and $LuPO_4:Ce^{3+}$ (2,4) under X-ray excitation.

Luminescence decay kinetics

The luminescence decay kinetics of $Lu_xY_{1-x}PO_4:Ce^{3+}$ under VUV energy excitation ($E_{ex.}$= 15.5 eV) are presented in fig. 15. The decay kinetics curves of $LuPO_4:Ce^{3+}$ and $YPO_4:Ce^{3+}$ have a single exponential shape whereas the mixed phosphates are fitted by two exponential functions (see table 2). The decay time

τ_2 = 17-25 ns is a characteristic time for the decay of Ce^{3+} emission which is peaking in the UV spectral region (320-360 nm in the case of the studied mixed phosphates). Presence of additional faster component in the decay with τ_1 = 5-11 ns is not characteristic for the 5d-4f radiative transitions of the Ce^{3+} ion. It can be connected with the partial quenching of Ce^{3+} emission. This conclusion is supported by the decrease of Ce^{3+} emission intensity in mixed phosphates with intermediate **x** values (fig.13, inset). The fastest decay times were detected for the intermediate value of **x** = 0.5. The acceleration of decay is also attributed to the quenching process because this sample demonstrates the lowest intensity of luminescence under both VUV and X-ray excitation.

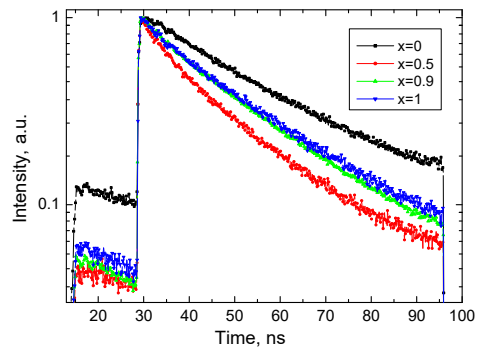

Figure 15. The decay kinetics of Ce^{3+} emission for the $Lu_xY_{1-x}PO_4:Ce^{3+}$ under VUV excitation (E_{ex} = 15.5 eV), T=300 K.

Table 2. The fitting parameters of the luminescence decay kinetics for the $Lu_xY_{1-x}PO_4:Ce^{3+}$ under VUV excitation (E_{ex} = 15.5 eV). The fit was performed by a function $y = y_0 + A_1 * e^{-\frac{x}{t_1}}$ for **x** = 0, **x** = 1, and $y = y_0 + A_1 * e^{-\frac{x}{t_1}} + A_2 * e^{-\frac{x}{t_2}}$ for **x** = 0.5, **x** = 0.9 (τ_1, τ_2 are the luminescence decay times in ns, A_1, A_2 – amplitudes, y_0 – is the level of the contribution of slow components to the luminescence decay kinetics).

x value	τ_1	A_1	τ_2	A_2	y_0
0	-	-	25.1	3.1	0.09
0.5	4.3	211.5	18.9	3.4	0.04
0.9	4.9	56.6	22.8	3.04	0.03
1	–	–	20	3.9	0.06

Luminescence excitation spectra

The time-resolved excitation spectra of $Lu_xY_{1-x}PO_4:Ce^{3+}$ are shown in fig. 16. The spectra consist of five luminescence bands in the energy range from 3.5 to 6.5 eV, which are attributed to the 4f-5d transitions of the Ce^{3+} ions. With the increase of **x** value the bands gradually shift to lower energies that is associated with a decrease of the lattice constants. At higher excitation energies the broad

peak with maximum at 8 eV is observed in excitation spectra measured in both fast and slow time windows. The peak is due to the photoionization of Ce^{3+} centers when the hole remains at Ce ion while the electron is excited into the conduction band. The process results in the delay of the recombination on Ce^{3+}. The gradual increase of intensity starting from the fundamental absorption edge at ~ 9 eV is detected. In this region the excitation of Ce^{3+} doped phosphates can be realized via two channels. The first one follows the scheme (I): (e+h – «ex» – $Ce^{3+(*)}$ – Ce^{3+} + $h\nu$), the second one follows the scheme (II): Ce^{3+}+ h – Ce^{4+} + e – $Ce^{3+(*)}$ – Ce^{3+} + $h\nu$ [17]. In the first case an electron and a hole create an exciton, which is captured by the luminescence center with subsequent emission of the luminescence quantum. In the second case the Ce^{3+} ions are excited by consecutive capture of a hole and then of an electron. The exciton peak was not detected on the fundamental absorption edge in the $Lu_xY_{1-x}PO_4:Ce^{3+}$. Therefore, the energy transfer to Ce^{3+} is realized by the scheme (II).

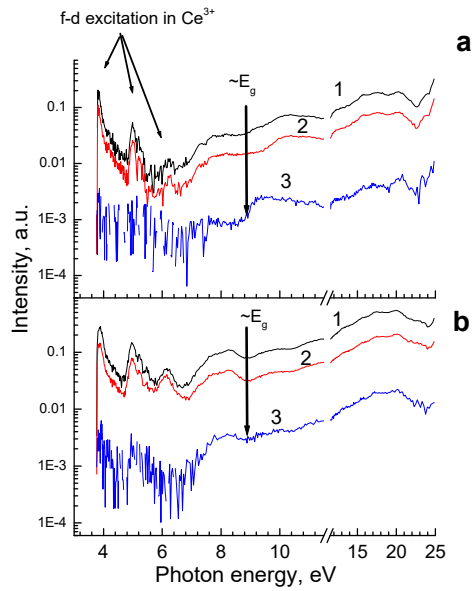

Figure 16. The time-resolved luminescence excitation spectra of $LuPO_4:Ce^{3+}$ (a) and $YPO_4:Ce^{3+}$ (b) measured in the integrated mode (1) and fast (2) and slow (3) time windows, λ_{em} = 365 nm (a), T=7 K.

The time-resolved spectroscopy allows to separate the fast and slow processes in the energy transfer from the host to the Ce^{3+} ions. The intracenter excitation of the Ce^{3+} ions and excitation via excitons are referred to the fast ones. The slow process is referred to the excitation of the Ce^{3+} ions by the capture of electron in case of photoionization of Ce^{3+} ions or by the consecutive capture of separated electron-hole pairs. The latter process reveals itself when the electrons

and holes are separated, i.e. above the bandgap. Therefore, the onset of intensity increase in the excitation spectrum in slow time windows allows to estimate the bandgap value. For the $YPO_4:Ce^{3+}$ the increase of slow component starts from 8.6-8.7 eV, and this threshold shifts up to 8.8-8.9 eV for $LuPO_4:Ce^{3+}$. This estimation confirms the conclusions on the bandgap estimations obtained on the basis of the analysis of luminescence excitation spectra of undoped phosphates (see section 5.2.1, fig.12).

5.2.3. Luminescence properties of $Lu_xY_{1-x}PO_4:Eu^{3+}$

The luminescence of $Lu_xY_{1-x}PO_4:Eu^{3+}$ solid solutions is ascribed to the 4f-4f transitions of the Eu^{3+} ions at 300 K. (fig. 17). At low temperatures an additional broad defect-related emission band in the range 300-550 nm was detected as well. The most intensive emission of Eu^{3+} at 300 K was detected for samples with **x** = 0.1 and **x** = 0.7 (fig. 17, inset).

Temperature dependence of luminescence

The temperature dependences of the luminescence intensity of $Lu_xY_{1-x}PO_4:Eu^{3+}$ under X-ray excitation are presented in fig. 18. For the defect-related emission the temperature quenching is observed starting from 100 K (fig. 18b). The intensity decrease of the defect related emission correlates with the increase of the Eu^{3+} emission that indicates the competition in the radiative relaxation between these emission centers. The energy transfer to the Eu^{3+} at higher temperature is more probable then to the defect center. Also according to the detected TSL peaks, the traps reveal themselves in the temperature range 150-450 K (see section 5.2.4 and publication II). The traps create additional energy relaxation channels, which influence the temperature dependence of the Eu^{3+} luminescence intensity. With the increase of temperature the charge carriers are released from the traps that allows their migration through the crystal lattice and increases probability to be captured by the Eu^{3+} ions. It is the reason for the intensity increase of Eu^{3+} emission in the range 180-450 K. The $Lu_xY_{1-x}PO_4:Eu^{3+}$ solid solutions with **x** = 0.1 and **x** = 0.7 demonstrate the best thermal stability in the 250-550 K range that correlates with the most intensive emission in these samples at room temperature (fig. 17). Therefore, the high temperature stability of the Eu^{3+} emission is associated with a lower concentration of traps in these samples.

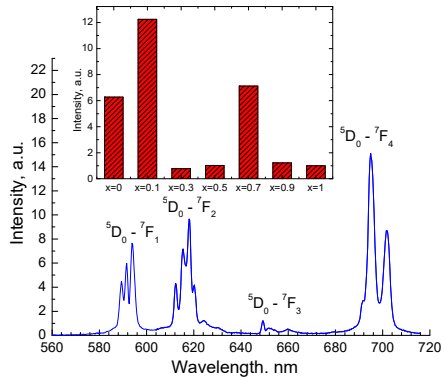

Figure 17. Luminescence spectrum of $Lu_{0.7}Y_{0.3}PO_4:Eu^{3+}$ under $E_{ex.}$ = 11.3 eV, T = 300 K. The inset shows the relative luminescence intensity of $Lu_xY_{1-x}PO_4:Eu^{3+}$ solid solutions under X-ray excitation, T = 300 K.

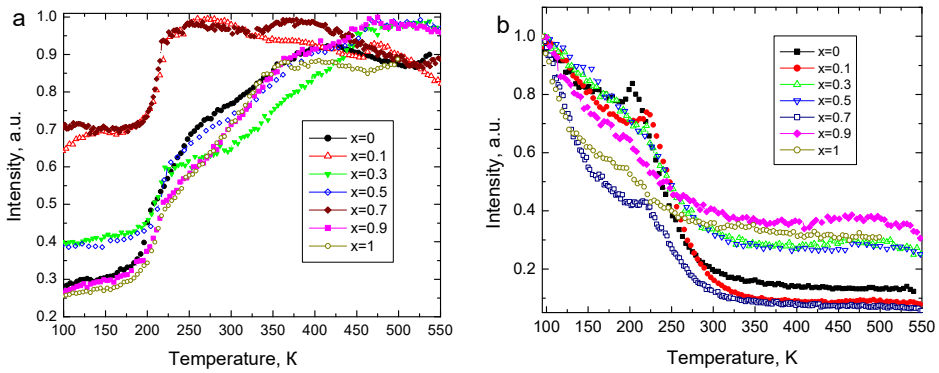

Figure 18. Temperature dependence of the Eu^{3+} (a) and defect (b) luminescence in the $Lu_xY_{1-x}PO_4:Eu^{3+}$ under X-ray excitation.

Luminescence excitation spectra

The luminescence excitation spectra of $Lu_xY_{1-x}PO_4:Eu^{3+}$ are presented in fig. 19. In the range below 4.5 eV the low-intensity narrow lines attributed to the 4f-4f transitions of the Eu^{3+} ions were observed (fig. 19a). The broad band with a maximum at 5.8 eV corresponds to the O-Eu charge transfer transitions. In the range below the fundamental absorption edge two distinctive peaks at 8.15 eV and 8.75 eV were detected (fig.19b). The first peak is ascribed to the Eu^{3+} intracenter 4f-5d transitions [37], while the second one is observed on the fundamental absorption edge and can be attributed to an exciton creation Also the position of peak at 8.75 eV coincides with the drop of intensity in the excitation spectrum of defect-related emission band, which is excited in transparency region of crystal (see fig. 19b and section 5.2.1).

In the region of the interband transitions ($E_{ex.}$ > 9 eV) the energy transfer from the host to the Eu^{3+} ions can be realized either via formation of excitons from the separated electron - hole pairs or consecutive capture of the electrons and holes by the Eu^{3+} ions (more details in section 5.2.2). The excitation band detected at the fundamental absorption edge (8.6-8.8 eV) is attributed to the energy transfer to the Eu^{3+} centers via direct creation of excitons. Usually the excitonic type of energy transfer to emission centers results in the intensity decrease in excitation spectra with the energy increase up to the edge of photon multiplication. However, after the excitonic peak the decrease of luminescence intensity was revealed only up to 11 eV and this energy is not sufficient to start the photon multiplication. Conversely, at $E_{ex.}$ > 11 eV the increase of intensity is observed that is the characteristic to the energy transfer by the scheme (II) (see introduction and section 5.2.2.). Therefore, both channels of energy transfer contribute to the formation of the excitation spectrum of the $Lu_xY_{1-x}PO_4:Eu^{3+}$ that is a favorable feature for the application in high energy conversion into visible light.

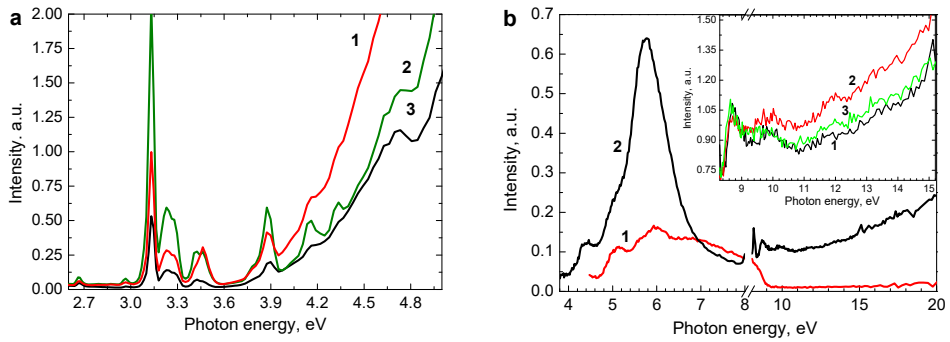

Figure 19. The luminescence excitation spectra of $Lu_xY_{1-x}PO_4:Eu^{3+}$ in the range:
(a) 2.5-4.0 eV, $\lambda_{em.}$ = 620 nm, **x** = 0.5 (curve 1), **x** = 0.3 (curve 2), **x** = 0.7 (curve 3);
(b) 4.0-20 eV, **x** = 0.9, $\lambda_{em.}$ = 420 nm (1), λ_{em} = 590 nm (2). The inset shows luminescence excitation spectra of $Lu_xY_{1-x}PO_4:Eu^{3+}$, normalized to energy E = 8.6 eV, λ_{em} = 590 nm for **x** = 0.9 (1), **x** = 0.5 (2), **x** = 0.3 (3), T = 300 K.

It is worth noting that in $Lu_xY_{1-x}PO_4:Eu^{3+}$ the efficiency of the energy transfer from the host to the Eu^{3+} ions in the energy range of interband transitions increases for intermediate **x** values (fig.19b, inset). When the excitation spectra are normalized to the intensity of the exciton peak at 8.6 eV a more pronounced rise of luminescence intensity is observed for the sample with **x** = 0.5 at E_{ex} > 10 eV, thus indicating the enhancement of the energy transfer efficiency to the luminescence centers. Such effect in solid solutions is ascribed to the limitation of the mean free path of the separated electrons and holes that increases the probability of being captured by the same Eu^{3+} ions. However, in the case of $Lu_xY_{1-x}PO_4:Eu^{3+}$ this effect is less pronounced than the trapping of the charge carriers and does not determine the formation of the luminescence intensity dependence on the **x** value (see fig.17, inset and discussion above).

5.2.4. Bandgap modification of $Lu_xY_{1-x}PO_4:RE^{3+}$ (RE =Ce, Eu)

The analysis of TSL peaks position (fig.20) revealed the effect of the relative concentration of Y and Lu cations in $Lu_xY_{1-x}PO_4$ on the band structure. In the phosphate solid solutions doped with Ce^{3+} ions a gradual shift of the TSL peaks with the increase of **x** values to higher temperature range was detected, that indicates increasing traps depth. The luminescence spectra of all TSL peaks originated from the Ce^{3+} emission, and the Ce^{3+} ions form stable hole traps [38]. Therefore, the position of TSL peaks in $Lu_xY_{1-x}PO_4:Ce^{3+}$ determines a depth of electron traps, and the shift of TSL peaks is connected with a move of the CB bottom. In the case of the phosphate solid solutions doped with Eu^{3+} ions the gradual shift of the TSL peaks was not observed. The luminescence spectra of TSL peaks originated only from the Eu^{3+} emission. Also the fact that Eu^{3+} ions in $Lu_xY_{1-x}PO_4:Eu^{3+}$ are stable electron traps [39] allowed to conclude that the observed peaks are associated with thermal release of holes. Therefore, the TSL peaks position is connected with the VB top. As a result, the study of TSL allowed to conclude that the electron states in the CB are shifted to higher energy range with increase of the **x** value. The changes of traps depth (activation energy) in the phosphate solid solutions were estimated to be $E_A \sim 0.2$ eV using fitting of the TSL curves by the first order decay approximation (more details in section 4.2.8 and publication II). Therefore, the bandgap of $Lu_xY_{1-x}PO_4$ increases by ~ 0.2 eV from YPO_4 to $LuPO_4$ due to the upward shift of the CB bottom only. The scheme of such modification of the band structure in the $Lu_xY_{1-x}PO_4$ is presented in fig. 21.

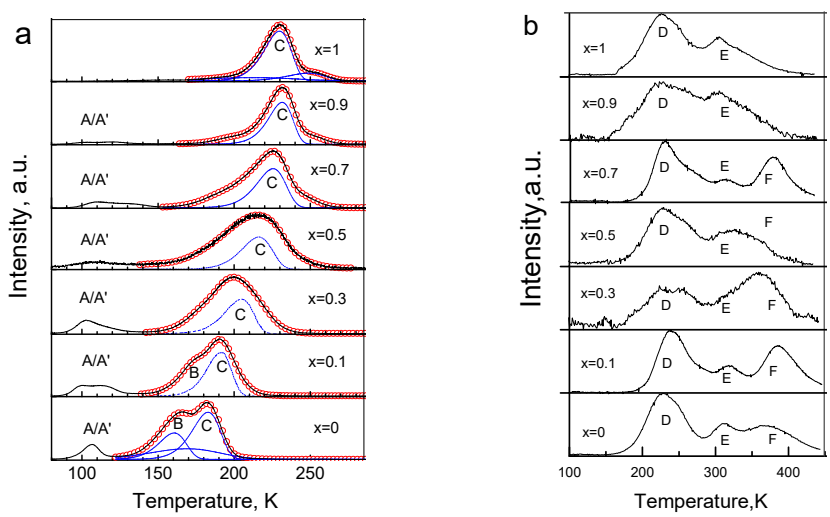

Figure 20. (a) The TSL curves of $Lu_xY_{1-x}PO_4:Ce^{3+}$ measured after irradiation with X-rays. The fitting of the curves is represented by red empty circles. The whole set of the elementary peaks used for the fitting is presented for compounds with **x** = 0 and 1, while for other compounds only the dominating peak C is presented for a better visualization; (b) The TSL curves of $Lu_xY_{1-x}PO_4:Eu^{3+}$ detected after irradiation with X-rays.

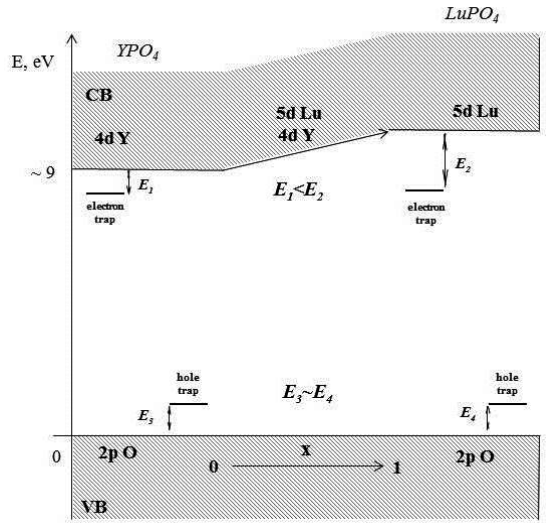

Figure 21. Scheme of the band structure of $Lu_xY_{1-x}PO_4$, which describes the band shift with **x** value.

5.3. Borate solid solutions

The crystal structure and phase composition of all borates solid solutions were studied by the XRD method. It was determined that the lattice constants gradually decrease with the increase of **x** value. Also the second calcite crystal phase for $Lu_xY_{1-x}BO_3:Ce^{3+}$ with $\mathbf{x} \geq 0.5$ and for $Lu_xY_{1-x}BO_3:Eu^{3+}$ with $\mathbf{x} \geq 0.75$ were revealed. The percentage of calcite phase in this case is not more than 5%. In the undoped $Lu_{0.65}Y_{0.35}BO_3$ the percentage is about 14 %.

The luminescence properties of the undoped $LuBO_3$, $Lu_{0.65}Y_{0.35}BO_3$, YBO_3 borates in the UV- and VUV- energy ranges under excitation by SR were studied. Up to four luminescence bands at 260, 290, 350, 450 nm were detected under selective excitation (more details in publication IV). The UV-luminescence at 260 nm was attributed to the emission of STEs, which electron component localizes at *d*-levels of cations. The additional UV-luminescence band at 290 nm and the luminescence band in the visible range are connected with different centers of crystal structure defects.

The luminescence of $Lu_xY_{1-x}BO_3:Eu^{3+}$ consists of the set of narrow bands in the 575-720 nm range and corresponds to the $^5D_0$-^7F_j (j = 0,1,2,3,4) transitions of the Eu^{3+} ions (fig.22). It is worth noting that the shape of luminescence spectrum of the samples with two phases depends on the excitation energy.

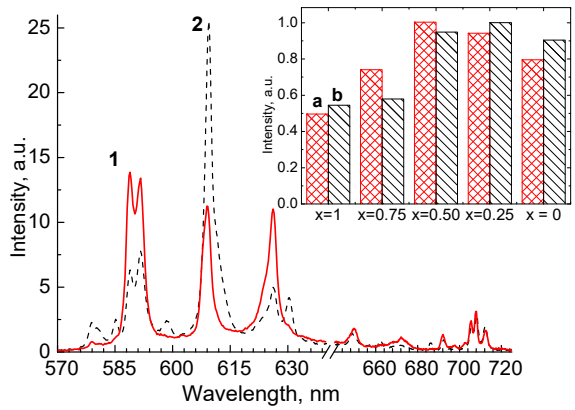

Figure 22. The luminescence spectra of $Lu_{0.75}Y_{0.25}BO_3:Eu^{3+}$ at $E_{ex.}$ = 5.4 eV (1) and 5.9 eV (2), T = 300 K. The inset shows the relative luminescence intensity of $Lu_xY_{1-x}BO_3:Eu^{3+}$ at $E_{ex.}$ = 11 eV (a) and X-ray $E_{ex.}$ = 30 keV (b).

Under interband excitation (E_{ex} > 9 eV) the increase of the Eu^{3+} luminescence intensity in $Lu_xY_{1-x}BO_3:Eu^{3+}$ was detected (fig.22, inset). One of explanations of this effect is an enhancement of the energy transfer efficiency to the luminescence centers by the separated electron-hole pairs. It can be explained by the limitation of the migration distance between the thermalized genetic electron-hole pairs in the solid solutions. (fig.23). However, in the energy region below 8 eV the intensity of $Lu_xY_{1-x}BO_3:Eu^{3+}$ excitation spectra for samples with two crystal phases decreases, that indicates a lowered efficiency of the energy transfer from the host to the Eu^{3+} ions. It was concluded that the presence of the second phase is the main factor affecting the luminescence intensity in $Lu_xY_{1-x}BO_3:Eu^{3+}$.

The luminescence spectra of $Lu_xY_{1-x}BO_3:Ce^{3+}$ solid solutions are presented in fig.24. The emission consists of the doublet with maxima at 380 and 420 nm, which are attributed to the 5d-4f transitions of the Ce^{3+} ions. With the increase of the **x** value the luminescence bands shift to longer wavelengths range due to the changes of the crystal field strength experienced by the Ce^{3+} ions. The Ce^{3+} luminescence intensity gradually decreases with the increase of **x** value because of the CB bottom modification.

Based on the analysis of TSL curves and the excitation spectra in the region of the intracenter Ce^{3+} excitation (E_{ex} < 8 eV) of the Ce^{3+} ion, it was shown that the width of bandgap decreases with the increase of **x** value. In this case, the position of the excited 5d levels of cerium gradually moves towards the CB bottom, which results in a thermal ionization of the Ce^{3+} ions and decrease of the luminescence intensity (more details in publication III).

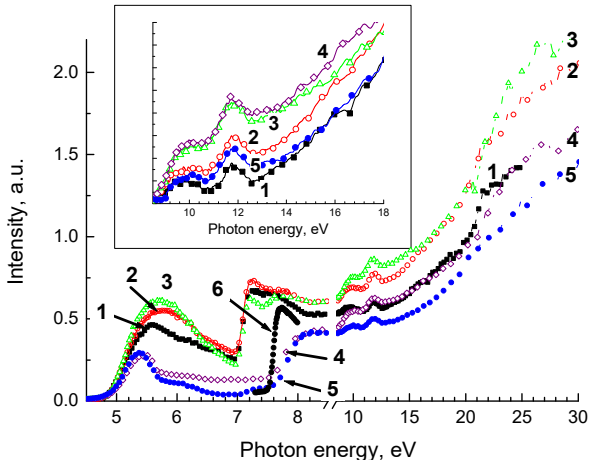

Figure 23. The luminescence excitation spectra of $Lu_xY_{1-x}BO_3:Eu^{3+}$ in the 4.5-30 eV energy range, $\lambda_{em.}$ = 590 nm, T = 300 K for **x** = 0 (1), 0.25 (2), 0.50 (3), 0.75 (4), and 1 (5), the excitation spectrum of STEs emission in YBO_3 at $\lambda_{em.}$= 260 nm, T = 10 K (6), and the excitation spectrum of $Lu_{0.75}Y_{0.25}BO_3:Eu^{3+}$ at $\lambda_{em.}$ = 610 nm, T = 300 K (7). The inset shows the excitation spectra of $Lu_xY_{1-x}BO_3:Eu^{3+}$ normalized to E = 8.2 eV.

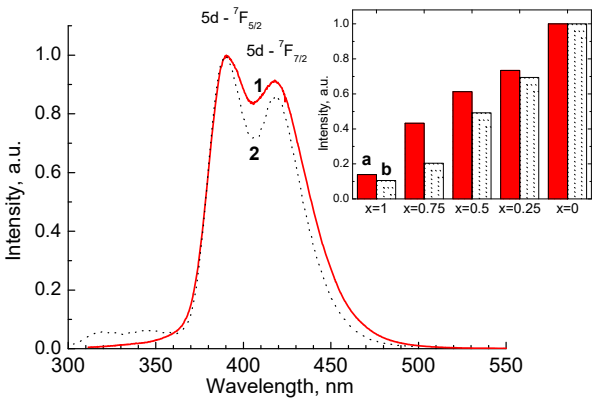

Figure 24. The luminescence spectrum of $Lu_{0.5}Y_{0.5}BO_3:Ce^{3+}$ $E_{ex.}$ = 11 eV (1) and 130 eV (2), T=300 K. The inset shows the relative intensity of $Lu_xY_{1-x}BO_3:Ce^{3+}$ at $E_{ex.}$ = 11 eV (a) and 130 eV (b).

SUMMARY

The main goal of the thesis was to determine the influence of the electronic structure, phase composition and the limitation of charge carriers free path on the luminescence properties and, in particular, on the processes of energy transfer from the host to the luminescence centers of the undoped and doped with the Eu^{3+} or Ce^{3+} ions solid solutions of $Lu_xY_{1-x}VO_4$, $Lu_xY_{1-x}PO_4$, and $Lu_xY_{1-x}BO_3$. The following results were obtained.

1) It was shown that $Lu_xY_{1-x}PO_4$ and $Lu_xY_{1-x}VO_4$ are homogeneous, single-phase, well-structured compounds with the tetragonal space group I41/amdZ, the structure type of xenotime. $Lu_xY_{1-x}BO_3$ crystallize in the structural type of vaterite for $\mathbf{x} < 0.5$, while additional calcite phase was detected for the solid solutions with $\mathbf{x} \geq 0.5$ for $Lu_xY_{1-x}BO_3:Ce^{3+}$ and with $\mathbf{x} \geq 0.75$ for $Lu_xY_{1-x}BO_3:Eu^{3+}$. The calcite phase content was not more than 5% in the doped borates. It was shown that the lattice constants of the vanadates, phosphates, and borates solid solutions decrease and follow Vegard's law with the increase of **x** value.
2) The luminescence band at 440-475 nm in the undoped vanadate $Lu_xY_{1-x}VO_4$ is caused by the self-trapped excitons emission. It was shown that the bandgap value of solid solutions is 3.5-3.6 eV and it negligibly depends on the **x** value, that indicates the formation of the valence band and the conduction band by the electronic states of oxyanion complex. The nonlinear dependence of the luminescence intensity in $Lu_xY_{1-x}VO_4$ at 300 K with a maximum of $\mathbf{x} = 0.7$ at 300 K was observed. It was shown that the luminescence is partially quenched at 300 K. The quenching temperature depends on the **x** value and determines the luminescence intensity of undoped $Lu_xY_{1-x}VO_4$.
3) The most intensive emission in $Lu_xY_{1-x}VO_4:Eu^{3+}$ was detected for $\mathbf{x} = 0.3$ and $\mathbf{x} = 0.7$ at T=300 K. It was shown that in $Lu_xY_{1-x}VO_4:Eu^{3+}$ the efficiency of energy transfer from the host to the luminescence centres increases for intermediate **x** value that is determined by the charge carriers free path limitation in the solid solution.
4) It was shown that the emission bands at 365, 415, and 445 nm in $Lu_xY_{1-x}PO_4$ are related to the luminescence centres formed by crystal defects, whereas the intrinsic luminescence of self-trapped excitons was not observed down to 5 K.
5) The bandgap value of $Lu_xY_{1-x}PO_4$ increases from 8.6-8.7 to 8.8-8.9 eV with increase of **x** value from 0 to 1. The origin of the modification of bandgap with **x** value was studied using the data on the electron and hole traps activation energies obtained by the thermally stimulated luminescence method. It is shown that the bandgap value increase is due to the upward shift of electron states of the conduction band bottom.

6) It was shown that the dependence of the 4f-4f Eu^{3+} luminescence intensity in $Lu_xY_{1-x}PO_4:Eu^{3+}$ on the **x** value is predominantly defined by competition between the Eu^{3+} luminescence centres and deep traps.
7) It was shown that the luminescence band at 260 nm of the undoped borates can be attributed to the self-trapped excitons, while the bands at 290, 350 and 450 nm are related to the luminescence centres formed by crystal defects. The bandgap of borate solid solutions was estimated as 7.5-7.8 eV.
8) The luminescence of $Lu_xY_{1-x}BO_3:Ce^{3+}$ and $Lu_xY_{1-x}BO_3:Eu^{3+}$ solid solutions is connected with the 5d-4f transitions of the Ce^{3+} and 4f-4f transitions of the Eu^{3+} ions, respectively. The luminescence intensity gradually decreases with the increase of **x** value in $Lu_xY_{1-x}BO_3:Ce^{3+}$ that is due to the modification of bandgap and the increase of the probability of the thermal ionization of the Ce^{3+} 5d states. The increase of luminescence intensity for the intermediate **x** values in $Lu_xY_{1-x}BO_3:Eu^{3+}$ was detected, that is connected with a cumulative effect of the charge carriers free path limitation and the adverse influence of calcite phase on the energy transfer from the host to the Eu^{3+} ions in the samples with $\mathbf{x} \geq 0.75$.

SUMMARY IN ESTONIAN

Energiaülekande protsessid kompleksete oksiidide segukristallides

Käesoleva doktoritöö eesmärgiks oli uurida elektroonstruktuuri, faasikoostisest ja laengukandjate vabatee piiratuse mõju luminestsentsomadustele. Erilise tähelepanu all oli energia ülekanne luminestsentstsentritele lisandamata ja Eu^{3+} või Ce^{3+} ioonidega lisandatud $Lu_xY_{1-x}VO_4$, $Lu_xY_{1-x}PO_4$, ja $Lu_xY_{1-x}BO_3$ segukristallides. Töö raames koguti järgnevad tulemused.

1. Näidati, et $Lu_xY_{1-x}PO_4$, ja $Lu_xY_{1-x}VO_4$ on homogeensed ja faasipuhtad ühendid ksenotiimi struktuuriga ja kuuluvad tetragonaalsesse ruumirühma I41/amdZ. $Lu_xY_{1-x}BO_3$ kristalliseerub vateriidi struktuuri kui $x < 0.5$, kusjuures kaltsiidi lisafaas leiti kui $\mathbf{x} \geq 0.5$ ja $\mathbf{x} \geq 0.75$ vastavalt $Lu_xY_{1-x}BO_3:Ce^{3+}$ ja $Lu_xY_{1-x}BO_3:Eu^{3+}$ jaoks. Kaltsiidi faasi osakaal oli vähem kui 5% lisandatud boraatides. Leiti, et vanadaatide, fosfaatide ja boraatide segukristallides võreparameetrid vähenevad ja järgivad Vegardi seadust **x** väärtuse kasvades.
2. Luminestsentsi riba 440-475 nm juures lisandamata vanadaadis $Lu_xY_{1-x}VO_4$ on põhjustatud iselõksustunud eksitonide rekombinatsioonist. Keelutsooni laius segukristallides oli 3.5-3.6 eV ja see sõltus vähesel määral x väärtusest, mis näitab, et valentstsoon ja juhtivustsoon koosnevad oksüanioni kompleksi elektroonsetest seisunditest. Täheldati iselõksustunud eksitoni luminestsentsi intensiivsuse mittelineaarset sõltuvust x-st, maksimumiga $\mathbf{x} = 0.7$ juures, $Lu_xY_{1-x}VO_4$ segukristallis 300K juures. Näidati, et see luminestsents on osaliselt kustutatud 300 K juures, kus temperatuurne kustumine sõltub **x** väärtusest.
3. Kõige tugevamat luminestsentsi intensiivsust registreeriti $Lu_xY_{1-x}VO_4:Eu^{3+}$ segukristalli jaoks $\mathbf{x} = 0.3$ ja $\mathbf{x} = 0.7$ väärtuste korral 300 K juures. Energia ülekande efektiivsus maatriksilt luminestsentstsentrile kasvab keskmiste **x** väärtuste jaoks segukristallis $Lu_xY_{1-x}VO_4:Eu^{3+}$, mis on määratud laengukandjate vabatee piiratusega segukristallides.
4. Kiirgusribad 365, 415 ja 445 nm juures on seotud defektide luminestsentstsentritega segukristallis $Lu_xY_{1-x}PO_4$, kui samas iselõksustunud eksitoni kiirgust ei täheldatud ka 5 K juures.
5. Keelutsooni laius kasvab väärtustelt 8.6-8.7 eV väärtusteni 8.8-8.9 eV kui **x** väärtus kasvab vahemikus 0 kuni 1. Keelutsooni laiuse muutuse sõltuvust **x** väärtusest uuriti $Lu_xY_{1-x}PO_4$ segukristallides kasutades aktivatsioonienergiaid elektronide ja aukude lõksude jaoks, mis arvutati termostimuleeritud luminestsentsi andmetest. Näidati, et keelutsooni laienemine on põhjustatud juhtivustsooni elektroonsete seisundite nihkest kõrgematele energiatele.
6. 4f-4f Eu^{3+} luminestsentsi intensiivsuse sõltuvus väärtusest **x** segukristallis $Lu_xY_{1-x}PO_4:Eu^{3+}$ on põhiliselt määratud konkureerivate protsessidega Eu^{3+} luminestsents-tsentrite ja sügavate lõksude vahel.

7. Luminestsensi kiirgusriba 250 nm juures seostati iselõksustunud eksitonidega lisandamata boraatides. Kiirgusribad 290, 350 ja 450 nm juures on seotud defekti tsentrite luminestsentsiga. Boraatide segukristallide keelutsooni laiuseks hinnati 7.5-7.8 eV.
8. Luminestsents $Lu_xY_{1-x}BO_3:Ce^{3+}$ ja $Lu_xY_{1-x}BO_3:Eu^{3+}$ segukristallides on seotud vastavalt Ce^{3+} 5d-4f üleminekuga ja Eu^{3+} 4f-4f üleminekuga. Luminestsentsi intensiivsus väheneb järk-järgult **x** väärtuse suurenemisega $Lu_xY_{1-x}BO_3:Ce^{3+}$ segukristallis, mis on seotud keelutsooni muutusega ja Ce^{3+} 5d olekute termilise ionisatsiooni tõenäosuse suurenemisega. Leiti, et luminestsentsi intensiivsuse suurenemine keskmiste **x** väärtuste juures $Lu_xY_{1-x}BO_3:Eu^{3+}$ segukristallides on seotud laengukandjate vaba tee piiratuse ja kaltsiidi faasi ebasoodsa mõju koosmõjuga energiaülekandele põhiainelt Eu^{3+} ioonidele segukristallides, kus $\mathbf{x} \geq 0.75$.

ACKNOWLEDGEMENTS

I am very grateful to my supervisors Dr. D. Spassky and Prof. M.G. Brik for their constant support and guiding me during my PhD study to complete this thesis.

I am very thankful to all my colleagues of the laboratory of Physics of Ionic Crystals for providing a friendly and fruitful working atmosphere. Special thanks to Ivo Romet, Dr. Vitali Nagirnyi, Dr. Eduard Aleksanyan, Eliko Tõldsepp for help with the measurements at the Institute of Physics in Tartu; Dr. Andrey Belsky and Dr. Sergii Gridin for the carrying out the measurements with the X-ray excitation source at the Institute of Light and Matter, University of Claude Bernard Lyon 1; Dr. Elena Samsonova for fruitful discussions and friendly support; Prof. Andrey Vasil'ev for discussion of the experimental results, Dr. Marco Kirm for support during all period of my PhD study and, especially, at the LUMINET meetings.

I am grateful to Anna Madej and Prof. Eugeniusz Zych for the supervision and new skills I acquired on synthesis and crystal structure study at the Faculty of Chemistry, University of Wroclaw; Dr. Karol Bartosiewicz and Prof. Martin Nikl for help with the measurements and analysis of experimental results at the Institute of Physics, Czech Academy of Science in Prague.

I am thankful to my family and friends for their support and understanding.

This study has been supported by the Curie Initial Training Network LUMINET (grant agreement no. 316906). I also acknowledge a partial financial support from the Estonian Centre of Excellence TK141 by the EU through the European Regional Development Fund (TK141 "Advanced materials and high-technology devices for energy recuperation systems", project No. 2014-2020.4.01.15-0011), the Graduate School of Functional Materials and Technologies, receiving funding from the European Regional Development Fund under project in University of Tartu.

REFERENCES

[1] М.Е. Глобус, Б.В. Гринев. *Неорганические сцинтилляторы. Новые и традиционные материалы* (Харьков: Акта, 2000).

[2] М.В. Коржик. *Физика сцинтилляторов на основе кислородных монокристаллов* (Мн.: БГУ, 2003).

[3] *Phosphor handbook. Ed. under the auspices of the Phosphor Research* (Society, Boca Raton: CRC Press, 1999).

[4] P. Lecoq, A. Annenkov, A. Gektin, M. Korzhik, Ch. Pedrini. *Inorganic Scintillators for Detector Systems* (Heidelberg, Germany: Springer, 2006).

[5] M.Fasoli, A.Vedda, M.Nikl, C. Jiang, B.P. Uberuaga, D.A. Andersson, K.J. McClellan, C.R. Stanek, *Phys. Rev. B* **84**, 081102 (2011).

[6] S. K. Yadav, B. P. Uberuaga, M. Nikl, C. Jiang, C. R. Stanek, *Phys. Rev. Appl*. **4**, 054012 (2015).

[7] A.N. Belsky, E. Auffray, P. Lecoq, C. Dujardin, N. Garnier, H. Canibano, C. Pedrini, A.G. Petrosyan, *IEEE Tran. Nucl. Science* **48**, 1095–1100 (2001).

[8] Y.O. Sidletskiy, V. Kononets, K. Lebbou, S. Neicheva, O. Voloshina, V. Bondar, V. Baumer, K. Belikov, A. Gektin, B. Grinyov, M.-F. Joubert, *Materials Research Bulletin* **47**, 3249–3252 (2012).

[9] O. Sidletskiy A. Belsky, A. Gektin, S. Neicheva, D. Kurtsev, V. Kononets, C. Dujardin, K. Lebbou, O. Zelenskaya, V. Tarasov, K. Belikov, B. Grinyov, *Gryst. Growth Des* **12**, 4411–4416 (2012).

[10] Y. Wu, D. Ding, S. Pan, F. Yang, G. Ren, *J. All. Comp.* **509**, 366–371 (2010).

[11] K. Kamada, T. Endo, K. Tsutumi, T. Yanagida, Y. Fujimoto, A. Fukabori, A. Yoshikava, J. Pejchal, M. Nikl, *Cryst. Grystal Des*. **11**, 4484–4490 (2011).

[12] G. Gundiah, K. Kamada, G. Bizarri, S. Hanrahan, M. Weber, E.Bourret-Courchesne, S. Derenzo, *NIM A* **652**, 234–237 (2011).

[13] D. Spassky, S. Omelkov, H. Mägi, V. Mikhailin, A. Vasil'ev, N. Krutyak, I. Tupitsyna, A. Dubovik, A. Yakubovskaya, A. Belsky, *Opt. Mat.* **36**, 1660–1664 (2014).

[14] A. N. Belsky, A. V. Gektin, S. N. Klimov, J. C. Krupa, P. Martin, A. Mayolet, V. Mikhailin, C. Pedrini, A. N. Vasil'ev, E. I. Zinin. Solid solutions of scintillators: A way of improving properties. // Proc. Int. Conf. Inorganic Scintillators and Their Applications (the Netherlands, 384–387, 1996).

[15] A.V. Gektin, A.N. Belsky, A.N. Vasilev, *IEEE Trans. Nucl. Sc*. **61**, 262–270 (2014).

[16] O. Sidletskiy, A. Gektin, A. Belsky, *Phys. Stat. Sol .A* **211** (10), 2384–2387 (2014).

[17] В.В. Михайлин, А.Н. Васильев. *Введение в спектроскопию твердого тела* (М: МГУ, 2010).

[18] A. Authier. *Early Days of X-ray Crystallography* (International Union of rystallography, Oxford University Press, 2013).

[19] В.И. Иверонова, А.А. Кацнельсон. *Ближний порядок в твердых растворах* (М.: Наука, 1977).

[20] А.Н. Бельский, Локализация и взаимодействие электронных возбуждений, созданных рентгеновским синхротронным излучением в неорганических сцинтилляторах. Диссерт. докт. ф.-м. наук, Москва 2000.

[21] Н.Р. Дудова, Р.О. Кайбышев, В.А. Валитов. *Физика металлов и металловедение* **108** (6), 657–666 (2009).

[22] В.В. Михайлин. *Синхротронное излучение в спектроскопии* (М.: Университетская книга, 2011).
[23] G. Zimmerer, *Rad. Meas*. **42**, 859–864 (2007).
[24] M.G. Brik, M. Bettinelli, E.Cavalli, *J. Sol. Stat. Chem*. **230**, 49–55 (2015).
[25] V. Pankratov, L. Grigorjeva, D. Millers, H. M. Yochum, *Phys. Status Solidi C* **4**, 801 (2007).
[26] C. Hsu, R. C. Powell, *J. Lumin*. **10**, 273–293 (1975).
[27] G. E. Venikouas, R. C. Powell, *J. Lumin.* **16**, 29–45 (1978).
[28] G. Blasse, A. Bril, *J. Chem. Phys*. **50**, 2974 (1969).
[29] M. Ya. Khodos, B. V. Shul'gin, F. F. Gavrilov, A. A. Fotiev, V. M. Lioznyanskii, *J. Appl. Spectroscopy* **16** (6), 758–761(1972).
[30] V. Panchal, D. Errandonea, A. Segura, P. Rodrı´guez-Hernandez, A. Munoz, S. Lopez-Moreno, M. Bettinelli, *J. Appl. Phys*. **110**, 043723 (2011).
[31] A. H. Krumpel, E. van der Kolk, E. Cavalli,P. Boutinaud, M. Bettinelli, P. Dorenbos, *J. Phys.: Condens. Matter* **21**, 115503 (2009).
[32] C. Zhi-Peng, W. Yu-Hua, Z. Jia-Chi, *Chin. Phys. B* **19** (5), 057803 (2010).
[33] M. R. Dolgos, A. M. Paraskos, M. W. Stoltzfus, S. C. Yarnell, P. M. Woodward, *J. Sol. St. Chem*. **182**, 1964–1971 (2009).
[34] V.N. Makhov, N.Yu. Kirikova, M. Kirm, J.C. Krupa, P. Liblik, A. Lushchik, Ch. Lushchik, E. Negodin, G. Zimmerer, *Nucl. Instrum. Methods Phys. Res. Sect. A* **486**, 437–442 (2002).
[35] V. Mikhailin, D.A. Spassky, V.N. Kolobanov, A.A. Meotishvili, D.G. Permenov, B.I. Zadneprovski, *Rad. Meas*. **45**, 307–310 (2010).
[36] T. Shalapska, P.Dorenbos, A. Gectin, G. Stryganyuk, A. Voloshinovskii, *J. Lumin.* **155**, 95–100 (2014).
[37] S. Hachani, B. Moine, A. El-akrmi, M. Ferid, *J. Lumin*. **130**, 1774–1783 (2010).
[38] H. Krumpel, A.J.J.Bos, A. Bessiere, E. Van der Kolk, P. Dorenbos, *Phys. Rev. B.* **80**, 085103 (2009).
[39] A. J.J. Bos, P. Dorenbos, A. Bessière, B. Viana, *Rad. Meas*. A **43**, 222–226 (2008).

PUBLICATIONS

CURRICULUM VITAE

Name: Viktoriia Levushkina
Date of birth: November 18, 1989
Nationality: Russian
Phone number: +372 5832 0343
E-mail: viktoriia.levushkina@ut.ee
Occupation: Phd student, University of Tartu, Institute of Physics, Tartu, Estonia

Education:

2013	M.Sc., M.V. Lomonosov Moscow State University, Department of Physics, Chair of optics and spectroscopy, Moscow, Russia.
2007	Physics and Technology school, Obninsk, Russia.

Languages: Russian, English.

Career:

2013–2016	Junior researcher, University of Tartu, Institute of Physics, Laboratory of Ionic Crystals, Tartu, Estonia.
03.17–06.17	Specialist, University of Tartu, Institute of Physics, Laboratory of Ionic Crystals, Tartu, Estonia.

Publications included in the thesis:

I. **Levushkina, V.S.**; Spassky, D.A.; Brik, M.G.; Zych, E.; Madej, A; Belsky, A.N; Bartosiewicz, K.; Nikl, M. Mixed vanadates: optimization of optical properties by varying chemical composition. Journal of Luminescence, in Press. DOI: 10.1016/j.jlumin.2016.12.009.

II. **Levushkina, V.S.**; Spassky, D.A.; Aleksanyan, E.M.; Brik, M.G.; Tretyakova, M.S.; Zadneprovski, B.I.; Belsky, A.N. Bandgap engineering of the $Lu_xY_{1-x}PO_4$ mixed crystals. Journal of Luminescence, 171; 2016, 33–39.

III. **Levushkina, V.S.**; Mikhailin, V.V.; Spassky, D.A.; Zadneprovski, B. I.; Tret'yakova, M.S. Luminescence properties of solid solutions of borates doped with rare-earths ions. Physics of the Solid State, 56(11); 2014, 2247–2258.

IV. Spassky, D.A.; **Levushkina, V.S.**; Mikhailin, V.V.; Zadneprovski, B. I.; Tret'yakova, M.S. Luminescence of Borates with Yttrium and Lutetium Cations. Physics of the Solid State, 55(1); 2013, 140–149.

Scholarships:

2013–2016	Marie Curie Initial Training Network LUMINET (grant agreement no. 316906).
2014–2017	PhD scholarship, University of Tartu.

ELULOOKIRJELDUS

Nimi: Viktoriia Levushkina
Sünniaeg: 18. november, 1989
Kodakondsus: Venelane
Telefon: +372 5832 0343
E-post: viktoriia.levushkina@ut.ee
Töökoht, amet: doktorandi üliõpilane, Füüsika Instituut, Tartu Ülikool, Tartu, Eesti

Haridus:

2013	M.Sc., Lomonossovi nimeline Moskva Riiklik Ülikool, füüsika osakond Moskva, Venemaa.
2007	Füüsikaline ja matemaatiline kool, Obninsk, Venemaa.

Keelteoskus: vene keel (emakeel), inglise keel (kõrgtase).

Töökogemus:

2013–2016	optika ja spektroskoopia nooremteadur, Tartu Ülikool, Füüsika Instituut, Tartu, Eesti.
03.17–06.17	spetsialist, Tartu Ülikool, Füüsika Instituut, Tartu, Eesti.

Teeside aluseks olevate publikatsioonide loetelu:

I. **Levushkina, V.S.**; Spassky, D.A.; Brik, M.G.; Zych, E.; Madej, A; Belsky, A.N; Bartosiewicz, K.; Nikl, M. Mixed vanadates: optimization of optical properties by varying chemical composition. Journal of Luminescence, in Press. DOI: 10.1016/j.jlumin.2016.12.009.

II. **Levushkina, V.S.**; Spassky, D.A.; Aleksanyan, E.M.; Brik, M.G.; Tretyakova, M.S.; Zadneprovski, B.I.; Belsky, A.N. Bandgap engineering of the $Lu_xY_{1-x}PO_4$ mixed crystals. Journal of Luminescence, 171; 2016, 33–39.

III. **Levushkina, V.S.**; Mikhailin, V.V.; Spassky, D.A.; Zadneprovski, B. I.; Tret'yakova, M.S. Luminescence properties of solid solutions of borates doped with rare-earths ions. Physics of the Solid State, 56(11); 2014, 2247–2258.

IV. Spassky, D.A.; **Levushkina, V.S.**; Mikhailin, V.V.; Zadneprovski, B. I.; Tret'yakova, M.S. Luminescence of Borates with Yttrium and Lutetium Cations. Physics of the Solid State, 55(1); 2013, 140–149.

Stipendiumid:

2013–2016	Marie Curie esmase koolituse võrgustik LUMINET.
2014–2017	doktorandi stipendium, Tartu Ülikool.

DISSERTATIONES PHYSICAE UNIVERSITATIS TARTUENSIS

1. **Andrus Ausmees.** XUV-induced electron emission and electron-phonon interaction in alkali halides. Tartu, 1991.
2. **Heiki Sõnajalg.** Shaping and recalling of light pulses by optical elements based on spectral hole burning. Tartu, 1991.
3. **Sergei Savihhin.** Ultrafast dynamics of F-centers and bound excitons from picosecond spectroscopy data. Tartu, 1991.
4. **Ergo Nõmmiste.** Leelishalogeniidide röntgenelektronemissioon kiiritamisel footonitega energiaga 70–140 eV. Tartu, 1991.
5. **Margus Rätsep.** Spectral gratings and their relaxation in some low-temperature impurity-doped glasses and crystals. Tartu, 1991.
6. **Tõnu Pullerits.** Primary energy transfer in photosynthesis. Model calculations. Tartu, 1991.
7. **Olev Saks.** Attoampri diapasoonis voolude mõõtmise füüsikalised alused. Tartu, 1991.
8. **Andres Virro.** AlGaAsSb/GaSb heterostructure injection lasers. Tartu, 1991.
9. **Hans Korge.** Investigation of negative point discharge in pure nitrogen at atmospheric pressure. Tartu, 1992.
10. **Jüri Maksimov.** Nonlinear generation of laser VUV radiation for high-resolution spectroscopy. Tartu, 1992.
11. **Mark Aizengendler.** Photostimulated transformation of aggregate defects and spectral hole burning in a neutron-irradiated sapphire. Tartu, 1992.
12. **Hele Siimon.** Atomic layer molecular beam epitaxy of A^2B^6 compounds described on the basis of kinetic equations model. Tartu, 1992.
13. **Tõnu Reinot.** The kinetics of polariton luminescence, energy transfer and relaxation in anthracene. Tartu, 1992.
14. **Toomas Rõõm.** Paramagnetic H^{2-} and F^+ centers in CaO crystals: spectra, relaxation and recombination luminescence. Tallinn, 1993.
15. **Erko Jalviste.** Laser spectroscopy of some jet-cooled organic molecules. Tartu, 1993.
16. **Alvo Aabloo.** Studies of crystalline celluloses using potential energy calculations. Tartu, 1994.
17. **Peeter Paris.** Initiation of corona pulses. Tartu, 1994.
18. **Павел Рубин.** Локальные дефектные состояния в CuO_2 плоскостях высокотемпературных сверхпроводников. Тарту, 1994.
19. **Olavi Ollikainen.** Applications of persistent spectral hole burning in ultrafast optical neural networks, time-resolved spectroscopy and holographic interferometry. Tartu, 1996.
20. **Ülo Mets.** Methodological aspects of fluorescence correlation spectroscopy. Tartu, 1996.
21. **Mikhail Danilkin.** Interaction of intrinsic and impurity defects in CaS:Eu luminophors. Tartu, 1997.

22. **Ирина Кудрявцева.** Создание и стабилизация дефектов в кристаллах KBr, KCl, RbCl при облучении ВУФ-радиацией. Тарту, 1997.
23. **Andres Osvet.** Photochromic properties of radiation-induced defects in diamond. Tartu, 1998.
24. **Jüri Örd.** Classical and quantum aspects of geodesic multiplication. Tartu, 1998.
25. **Priit Sarv.** High resolution solid-state NMR studies of zeolites. Tartu, 1998.
26. **Сергей Долгов.** Электронные возбуждения и дефектообразование в некоторых оксидах металлов. Тарту, 1998.
27. **Kaupo Kukli.** Atomic layer deposition of artificially structured dielectric materials. Tartu, 1999.
28. **Ivo Heinmaa.** Nuclear resonance studies of local structure in $RBa_2Cu_3O_{6+x}$ compounds. Tartu, 1999.
29. **Aleksander Shelkan.** Hole states in CuO_2 planes of high temperature superconducting materials. Tartu, 1999.
30. **Dmitri Nevedrov.** Nonlinear effects in quantum lattices. Tartu, 1999.
31. **Rein Ruus.** Collapse of 3d (4f) orbitals in 2p (3d) excited configurations and its effect on the x-ray and electron spectra. Tartu, 1999.
32. **Valter Zazubovich.** Local relaxation in incommensurate and glassy solids studied by Spectral Hole Burning. Tartu, 1999.
33. **Indrek Reimand.** Picosecond dynamics of optical excitations in GaAs and other excitonic systems. Tartu, 2000.
34. **Vladimir Babin.** Spectroscopy of exciton states in some halide macro- and nanocrystals. Tartu, 2001.
35. **Toomas Plank.** Positive corona at combined DC and AC voltage. Tartu, 2001.
36. **Kristjan Leiger.** Pressure-induced effects in inhomogeneous spectra of doped solids. Tartu, 2002.
37. **Helle Kaasik.** Nonperturbative theory of multiphonon vibrational relaxation and nonradiative transitions. Tartu, 2002.
38. **Tõnu Laas.** Propagation of waves in curved spacetimes. Tartu, 2002.
39. **Rünno Lõhmus.** Application of novel hybrid methods in SPM studies of nanostructural materials. Tartu, 2002.
40. **Kaido Reivelt.** Optical implementation of propagation-invariant pulsed free-space wave fields. Tartu, 2003.
41. **Heiki Kasemägi.** The effect of nanoparticle additives on lithium-ion mobility in a polymer electrolyte. Tartu, 2003.
42. **Villu Repän.** Low current mode of negative corona. Tartu, 2004.
43. **Алексей Котлов.** Оксианионные диэлектрические кристаллы: зонная структура и электронные возбуждения. Tartu, 2004.
44. **Jaak Talts.** Continuous non-invasive blood pressure measurement: comparative and methodological studies of the differential servo-oscillometric method. Tartu, 2004.
45. **Margus Saal.** Studies of pre-big bang and braneworld cosmology. Tartu, 2004.

46. **Eduard Gerškevitš.** Dose to bone marrow and leukaemia risk in external beam radiotherapy of prostate cancer. Tartu, 2005.
47. **Sergey Shchemelyov.** Sum-frequency generation and multiphoton ionization in xenon under excitation by conical laser beams. Tartu, 2006.
48. **Valter Kiisk.** Optical investigation of metal-oxide thin films. Tartu, 2006.
49. **Jaan Aarik.** Atomic layer deposition of titanium, zirconium and hafnium dioxides: growth mechanisms and properties of thin films. Tartu, 2007.
50. **Astrid Rekker.** Colored-noise-controlled anomalous transport and phase transitions in complex systems. Tartu, 2007.
51. **Andres Punning.** Electromechanical characterization of ionic polymer-metal composite sensing actuators. Tartu, 2007.
52. **Indrek Jõgi.** Conduction mechanisms in thin atomic layer deposited films containing TiO_2. Tartu, 2007.
53. **Aleksei Krasnikov.** Luminescence and defects creation processes in lead tungstate crystals. Tartu, 2007.
54. **Küllike Rägo.** Superconducting properties of MgB_2 in a scenario with intra- and interband pairing channels. Tartu, 2008.
55. **Els Heinsalu.** Normal and anomalously slow diffusion under external fields. Tartu, 2008.
56. **Kuno Kooser.** Soft x-ray induced radiative and nonradiative core-hole decay processes in thin films and solids. Tartu, 2008.
57. **Vadim Boltrushko.** Theory of vibronic transitions with strong nonlinear vibronic interaction in solids. Tartu, 2008.
58. **Andi Hektor.** Neutrino Physics beyond the Standard Model. Tartu, 2008.
59. **Raavo Josepson.** Photoinduced field-assisted electron emission into gases. Tartu, 2008.
60. **Martti Pärs.** Study of spontaneous and photoinduced processes in molecular solids using high-resolution optical spectroscopy. Tartu, 2008.
61. **Kristjan Kannike.** Implications of neutrino masses. Tartu, 2008.
62. **Vigen Issahhanjan.** Hole and interstitial centres in radiation-resistant MgO single crystals. Tartu, 2008.
63. **Veera Krasnenko.** Computational modeling of fluorescent proteins. Tartu, 2008.
64. **Mait Müntel.** Detection of doubly charged higgs boson in the CMS detector. Tartu, 2008.
65. **Kalle Kepler.** Optimisation of patient doses and image quality in diagnostic radiology. Tartu, 2009.
66. **Jüri Raud.** Study of negative glow and positive column regions of capillary HF discharge. Tartu, 2009.
67. **Sven Lange.** Spectroscopic and phase-stabilisation properties of pure and rare-earth ions activated ZrO_2 and HfO_2. Tartu, 2010.
68. **Aarne Kasikov.** Optical characterization of inhomogeneous thin films. Tartu, 2010.
69. **Heli Valtna-Lukner.** Superluminally propagating localized optical pulses. Tartu, 2010.

70. **Artjom Vargunin.** Stochastic and deterministic features of ordering in the systems with a phase transition. Tartu, 2010.
71. **Hannes Liivat.** Probing new physics in e+e− annihilations into heavy particles via spin orientation effects. Tartu, 2010.
72. **Tanel Mullari.** On the second order relativistic deviation equation and its applications. Tartu, 2010.
73. **Aleksandr Lissovski.** Pulsed high-pressure discharge in argon: spectroscopic diagnostics, modeling and development. Tartu, 2010.
74. **Aile Tamm.** Atomic layer deposition of high-permittivity insulators from cyclopentadienyl-based precursors. Tartu, 2010.
75. **Janek Uin.** Electrical separation for generating standard aerosols in a wide particle size range. Tartu, 2011.
76. **Svetlana Ganina.** Hajusandmetega ülesanded kui üks võimalus füüsikaõppe efektiivsuse tõstmiseks. Tartu, 2011
77. **Joel Kuusk.** Measurement of top-of-canopy spectral reflectance of forests for developing vegetation radiative transfer models. Tartu, 2011.
78. **Raul Rammula**. Atomic layer deposition of HfO_2 – nucleation, growth and structure development of thin films. Tartu, 2011.
79. **Сергей Наконечный.** Исследование электронно-дырочных и интерстициал-вакансионных процессов в монокристаллах MgO и LiF методами термоактивационной спектроскопии. Тарту, 2011.
80. **Niina Voropajeva.** Elementary excitations near the boundary of a strongly correlated crystal. Tartu, 2011.
81. **Martin Timusk.** Development and characterization of hybrid electro-optical materials. Tartu, 2012, 106 p.
82. **Merle Lust.** Assessment of dose components to Estonian population. Tartu, 2012, 84 p.
83. **Karl Kruusamäe.** Deformation-dependent electrode impedance of ionic electromechanically active polymers. Tartu, 2012, 128 p.
84. **Liis Rebane.** Measurement of the $W \to \tau\nu$ cross section and a search for a doubly charged Higgs boson decaying to τ-leptons with the CMS detector. Tartu, 2012, 156 p.
85. **Jevgeni Šablonin.** Processes of structural defect creation in pure and doped MgO and NaCl single crystals under condition of low or super high density of electronic excitations. Tartu, 2013, 145 p.
86. **Riho Vendt**. Combined method for establishment and dissemination of the international temperature scale. Tartu, 2013, 108 p.
87. **Peeter Piksarv.** Spatiotemporal characterization of diffractive and non-diffractive light pulses. Tartu, 2013, 156 p.
88. **Anna Šugai.** Creation of structural defects under superhigh-dense irradiation of wide-gap metal oxides. Tartu, 2013, 108 p.
89. **Ivar Kuusik.** Soft X-ray spectroscopy of insulators. Tartu, 2013, 113 p.
90. **Viktor Vabson**. Measurement uncertainty in Estonian Standard Laboratory for Mass. Tartu, 2013, 134 p.

91. **Kaupo Voormansik.** X-band synthetic aperture radar applications for environmental monitoring. Tartu, 2014, 117 p.
92. **Deivid Pugal.** hp-FEM model of IPMC deformation. Tartu, 2014, 143 p.
93. **Siim Pikker.** Modification in the emission and spectral shape of photostable fluorophores by nanometallic structures. Tartu, 2014, 98 p.
94. **Mihkel Pajusalu**. Localized Photosynthetic Excitons. Tartu, 2014, 183 p.
95. **Taavi Vaikjärv.** Consideration of non-adiabaticity of the Pseudo-Jahn-Teller effect: contribution of phonons. Tartu, 2014, 129 p.
96. **Martin Vilbaste.** Uncertainty sources and analysis methods in realizing SI units of air humidity in Estonia. Tartu, 2014, 111 p.
97. **Mihkel Rähn.** Experimental nanophotonics: single-photon sources- and nanofiber-related studies. Tartu, 2015, 107 p.
98. **Raul Laasner.** Excited state dynamics under high excitation densities in tungstates. Tartu, 2015, 125 p.
99. **Andris Slavinskis.** EST Cube-1 attitude determination. Tartu, 2015, 104 p.
100. **Karlis Zalite**. Radar Remote Sensing for Monitoring Forest Floods and Agricultural Grasslands. Tartu, 2016, 124 p.
101. **Kaarel Piip.** Development of LIBS for *in-situ* study of ITER relevant materials. Tartu, 2016, 93 p.
102. **Kadri Isakar.** ^{210}Pb in Estonian air: long term study of activity concentrations and origin of radioactive lead. Tartu, 2016, 107 p.
103. **Artur Tamm.** High entropy alloys: study of structural properties and irradiation response. Tartu, 2016, 115 p.
104. **Rasmus Talviste.** Atmospheric-pressure He plasma jet: effect of dielectric tube diameter. Tartu, 2016, 107 p.
105. **Andres Tiko.** Measurement of single top quark properties with the CMS detector. Tartu, 2016, 161 p.
106. **Aire Olesk.** Hemiboreal Forest Mapping with Interferometric Synthetic Aperture Radar. Tartu, 2016, 121 p.
107. **Fred Valk.** Nitrogen emission spectrum as a measure of electric field strength in low-temperature gas discharges. Tartu, 2016, 149 p.
108. **Manoop Chenchiliyan.** Nano-structural Constraints for the Picosecond Excitation Energy Migration and Trapping in Photosynthetic Membranes of Bacteria. Tartu, 2016, 115p.
109. **Lauri Kaldamäe.** Fermion mass and spin polarisation effects in top quark pair production and the decay of the higgs boson. Tartu, 2017, 104 p.
110. **Marek Oja.** Investigation of nano-size α- and transition alumina by means of VUV and cathodoluminescence spectroscopy. Tartu, 2017, 89 p.